**Abstract** We review the basic light-matter interactions and optical properties of chip-based single photon sources, that are enabled by integrating single quantum dots with planar photonic crystals. A theoretical framework is presented that allows one to connect to a wide range of quantum light propagation effects in a physically intuitive and straightforward way. We focus on the important mechanisms of enhanced spontaneous emission, and efficient photon extraction, using all-integrated photonic crystal components including waveguides, cavities, quantum dots and output couplers. The limitations, challenges, and exciting prospects of developing on-chip quantum light sources using integrated photonic crystal structures are discussed.

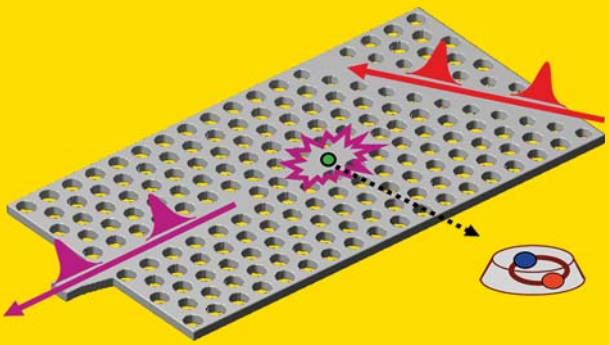

A sequence of optical pulses (top right) interacting with a single quantum dot embedded in a photonic crystal system, resulting in the emission of a train of single photons on-chip.



# On-chip single photon sources using planar photonic crystals and single quantum dots

*Peijun Yao* [1], *V. S. C. Manga Rao* [1,2], *and S. Hughes* [1,*]

[1] Department of Physics, Queen's University, Kingston, ON K7L 3N6, Canada
[2] present address: Department of Physics, University of Trento, 38100 Povo, Trento, Italy

Received: 23 December 2008, Revised: 21 April 2009, Accepted: 29 April 2009
Published online: 13 July 2009

**Key words:** Single photons, quantum dots, spontaneous emission, planar photonic crystals, cavity-QED, chip-based quantum optics, nanophotonics.

**PACS:** 42.50.Ct, 42.50.Pq, 42.70.Qs, 78.67.Hc

## 1. Introduction

There is currently a worldwide interest in the possibility of developing single photon sources, whose unique attributes have important applications in quantum information science and give rise to novel regimes of light-matter interaction. In particular, single photon sources could lead to practical ways of doing quantum computing [1], unconditional quantum cryptography [2], quantum communications systems [3], and "completely secure" data protection. Ideally, the quantum single-photon light source should emit strictly one photon at a time, where each photon is *indistinguishable* (cf. a train of photons), in a high repetition rate, thus functioning as a so called "photon gun." Although the single photon gun is a simple concept, producing trains of single photons "on demand" – or otherwise – is far from a trivial task, and many scientists have made strenuous attempts to achieve such a goal.

There are several established schemes that can facilitate the emission of single photons [4]. The easiest and most straightforward way is to attenuate pulsed lasers [5], though in this case the production of single photons is *probabilistic*. Therefore, there may be no photons, several photons, or many photons, since the photon number generated is subject to Poissonian statistics; this can be problematic for a number of applications such as quantum cryptography because of possible photon number-splitting *attacks* ("eavesdropping") [6, 7]. Another more practical approach for obtaining single photons is to exploit spontaneous parametric down conversion in nonlinear crystals [8], where higher-frequency pump photons incident on a nonlinear crystal are occasionally split into a pair of lower-frequency

* Corresponding author: e-mail: shughes@physics.queensu.ca

photons; one of these photons (the "heralding" photon) is used to herald the arrival of the second photon ("heralded" photon), and thus the second photon can be well isolated and manipulated. However, there is a contradiction problem here: a larger conversion rate is usually accompanied with a greater probability of emitting two photons, while a lower conversion rate will lead to the random production of single photons (although the probability of two photon emission can be effectively reduced).

Besides single photon emission from the above macroscopic material schemes, recently there has been extensive research devoted to *microscopic* structures, where an isolated quantum system functions as a source for the emitted photons. In theory, a single quantum object behaving as a two-level system is an ideal single photon emitter, and there are many possible candidates that may show such behaviour, including atoms [9, 10], ions [11], molecules [12, 13], and color centres [14]. In contrast to the low attenuated lasers and heralded schemes, the single photon emitter based on a single isolated quantum system can be *deterministic* and *on-demand*, since a single two-level system can emit precisely one photon each time it is excited. Yet, many of these isolated quantum systems are impractical for a number of reasons, and can suffer from photo-bleaching and blinking, or have problems that stem from their broad optical spectrum, since the real systems are much more complicated than an idealized two-level system.

From a practical perspective, semiconductor quantum dots (QDs) [15, 16] offer an attractive material system for emitting single photons. In part due to new design insights, and due to continued improvements in semiconductor fabrication technologies, many pioneering experiments using single QD-emitted photons are now coming to the fore. Some of advantages of the QDs include: large exciton dipole moments; integrable with compact semiconductor systems [17]; fixed in position and stable; compatible with electronics and lasers. Moreover, their excitonic emission spectra can be nano-engineered to cover ultraviolet, visible, and infrared frequencies, rendering them fully compatible with telecom sources and components. Most single photon sources based on QDs also have excellent emission efficiencies [18]. Self assembled QDs are nm-sized islands (typically about 20 nm in diameter and 3–5 nm in height), that are formed by having a smaller-bandgap semiconductor material embedded in a larger bandgap semiconductor material; for example, InAs embedded in GaAs. This leads to three-dimensional quantum confinement, and the electron and hole energy levels become discrete, similar to an atom. Consequently, QDs are commonly referred to an "artificial atoms"; one must keep in mind that QDs usually contain many thousands of atoms, but nevertheless they have energy levels that mimic the behavior of a two-level system.

Early optical experiments on semiconductor QDs demonstrated the well known two-level behaviour of Rabi flopping [21–23], where an excitation is driven from the ground state to the excited state and back again. However, the observed "flopping" behaviour is heavily damped, since semiconductor QDs suffer from the usual solid-state problems of environment-induced decoherence [24–27]. Decoherence has a major influence in the indistinguishable nature of the emitted photons, and is one of the biggest obstacles to overcome in realizing quantum information processing. Thus, most experiments performed to date work at cryogenic temperatures ($\sim 4$ K is typical), yet this alone is not enough to overcome the problems of decoherence. So one must somehow have the photon emitted fast enough (before the onset of decoherence becomes significant), which can be achieved by engineering the surrounding photon density of states that the QD sees. In this regard, it is now known that spontaneous emission of an atom or QD (photon emitter) can be strongly modified by the external dielectric environment due to the Purcell effect [28], which is an example of cavity-quantum electrodynamics (cavity-QED). This is precisely why the microcavities and inhomogeneous material systems are so important. In addition, to function as a practical photon source, efficient output collection of the photons (photon extraction) is necessary, and this is one of the major advantages of chip-based quantum emitters.

The first pioneering experiments to demonstrate QD-based single photons, were carried out with single InAs QDs embedded in semiconductor micropillars [29–32] and microdisks [18, 33], which are schematically shown in Fig. 1. These structures are grown by molecular beam epitaxy on a semi-insulating GaAs substrate, followed by etching around the target QD of interest. For the micropost example, the microcavity is sandwiched between two distributed Bragg reflectors (DBRs), where the reflectivity of the bottom DBR is designed to be significantly higher than that of the top DBR, so most of the light in the cavity escapes upwards. The single QD is contained within the cavity by selective etching, and the efficiency of the emitting single photons into an output propagation mode is found to be approximately 38%. For the microdisk, the enhancement of the spontaneous emission is achieved by coupling the QD to the high-quality whispering gallery modes (WGMs);

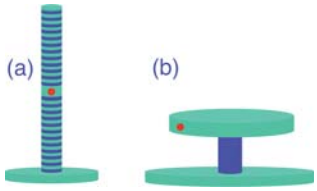


**Figure 1** (online color at: www.lpr-journal.org) Schematic diagram of two example single photon sources, based on a semiconductor micropost and a microdisk. (a) Micropost cavity sandwiched between two Bragg reflectors, where the QD is indicated by the red dot. In practise, a self-assembled QD would be more like a quantum dot disk, with excellent quantum confinement in the vertical (growth) direction. (b) Microdisk cavity with the WGMs spatially and spectrally coupled to target QD exciton. The QDs are typically distributed throughout the material, but only those close to the excited mode's antinodes (peak field points) can emit efficient single photons, while the contribution from the other dots can be approximately neglected.

although the QDs are distributed throughout the full disk, only those close to the excited mode's antinode field positions are effectively coupled to the target WGM, and thus the system could generate quasi single photon pulses at a repetition rate of around 1 GHz. In both cases, the Purcell factors are in the order of 10, which means that they emit photons ten times faster than the corresponding bulk material. Experimentally, the QDs are excited by a pulsed laser, and the quantum quality of the single photons – indistinguishability – is confirmed by measuring the antibunching behaviour of the second-order quantum correlation function, which is the standard experimental proof that no two photons can be emitted at the same time.

In this review, we focus our attention on several of the main design criteria that need to be addressed when developing single photon emitters from semiconductor QDs, and show the possible solution that planar photonic crystals (PCs) offer. The term photonic crystal was introduced by Yablonovitch [19] and John [20] in their seminal works in 1987. Photonic crystals are periodic composites that allow one to engineer how photons propagate, and semiconductor-based planar PCs are of particular interest due to their ease of fabrication using standard etching and lithography techniques. Some of the main questions that we attempt to address, include: *i*) How to realize a sufficiently large Purcell factor so that the effects of decoherence are minimized? *ii*) How to enable efficient photon extraction on-chip? *iii*) How to have large single-photon $\beta$ factors over a large bandwidth? *iv*) How to add in single photon functionality, such as the one photon switch? Throughout this review we discuss the underlying physics and skip the details of fabrication and experimental measurements, since these are described in many excellent experimental papers that are now appearing in the literature. In Sect. 2, we discuss the important measurement techniques commonly employed to probe single photon behaviour and efficiency. In Sect. 3, we introduce the general theory for describing the light-matter interactions and derive the exact electric field operator and the Purcell factor for arbitrary inhomogeneous dielectrics. In Sect. 4, we analyze the planar PC single cavity structure. In Sect. 5, we introduce the concept of open system cavity-QED, which is exemplified by studying the case of QD photon emission in a PC waveguide; both long waveguides and finite-size waveguides are analyzed; a connection to recent measurements is also established. In Sect. 6, we introduce practical on-chip single photon sources, by integrating couplers, cavities, and waveguides. In Sect. 7, we discuss the integrated side-coupled-cavity waveguide system, and introduce the phenomena of single photon switching and electromagnetic induced transparency. In Sect. 8, we give our conclusions and a brief outlook into the future.

## 2. Quantum statistics and measurement aspects of single photons

According to the photon time distribution, photon sources can be classified into three types: a) bunching, b) random, and c) antibunching; these distributions correspond to three varieties of photon number distribution, namely Bose-Einstein, Poisson, and sub-Poisson or *single photon* (see Fig. 2). These statistical properties can be accurately characterized by the second-order correlation function (or intensity correlation function) $g^{(2)}(\tau)$ – the conditional probability of detecting a photon at $t+\tau$, conditioned on detecting one at $t$. After normalizing by the average probability of emitting a photon at any time, one obtains the normalized second-order correlation function for stationary fields:

$$g^{(2)}(\tau) = \frac{\langle I(t)I(t+\tau)\rangle}{\langle I(t)\rangle^2}\,. \qquad (1)$$

Depending upon the source class, such as thermal (Bose-Einstein distribution) or coherent (Poisson distribution), the numerator in the above equation is always larger than the denominator: $\langle I^2\rangle \geq \langle I\rangle^2$, because any classical stationary random function of time must satisfy the Schwartz inequality, and so $g^{(2)}(\tau) \geq 1$. To describe the quantum property of a single photon source, one must use the second-order *quantum* correlation function [34, 35], defined as

$$g^{(2)}(t,\tau) = \frac{\langle :\, I(t)I(t+\tau)\, :\rangle}{\langle I(t)\rangle^2} = \frac{\langle \hat{a}^\dagger(t)\hat{a}^\dagger(t+\tau)\hat{a}(t+\tau)\hat{a}(t)\rangle}{\langle \hat{a}^\dagger(t)\hat{a}(t)\rangle^2}\,, \qquad (2)$$

where $\hat{a}^\dagger$ ($\hat{a}$) is the creation (annihilation) operators of the mode being measured and '::' denotes the normal ordering of the operators. For a sub-Poissonian source, such as the attenuated laser, $g^{(2)}(\tau=0) < 1$, which has a reduced multiphoton probability as compared to coherent light with Poissonian photon statistics. For a true single photon source, the value of $g^{(2)}(\tau=0) \to 0$, since two effective detection events for a single photon state $|1\rangle$ yields 0. Generally, the closer to $g^{(2)}(\tau=0) \to 0$, the better the single photon source, and this is a common experimental target.

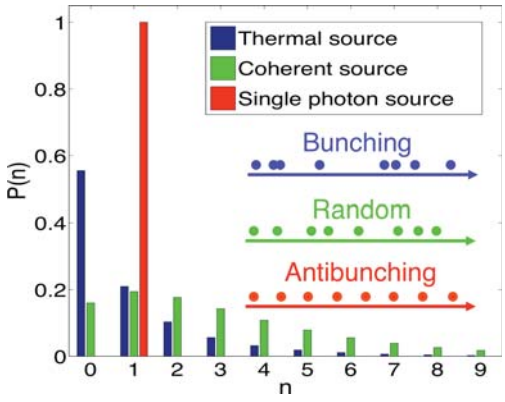


**Figure 2** (online color at: www.lpr-journal.org) The distribution of photon statistics for three different photon source types: thermal source, coherent source, and single photon source. The inset shows the time-dependence of the emitted photons corresponding to the three sources.

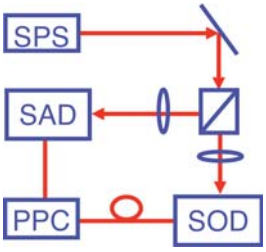


**Figure 3** (online color at: www.lpr-journal.org) Schematic experimental setup to measure the luminescence from a single photon source. SPS: single photon source, SAD: start detector, SOD: stop detector, PPC: photon-photon correlator.

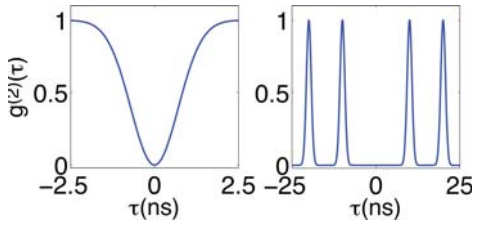


**Figure 4** (online color at: www.lpr-journal.org) Two examples of an ideal $g^{(2)}(\tau)$: (a) Continuous excitation and (b) pulse excitation.

With ideal detectors, $g^{(2)}(\tau)$ can be measured by simply recording the stream of photons with sufficient time-resolution, and then correlating the click events that happen at different time bins. Unfortunately, because of the re-loading time of the photomultiplier dynodes or semiconductor junction, real photon-counting detectors are inactive for a given length of time ("dead time") after detecting a photon; and current technology does not have photon-number resolving capabilities. An elegant solution to eliminate these factitious events and the dead time was first proposed by Hanbury Brown and Twiss [36, 37], which, interestingly, was originally developed to determine the angular radii of stars in astronomy. Coincidences between the two detectors are then insensitive to dead-times. The Hanbury Brown and Twiss setup is shown schematically in Fig. 3: the detection beam is split into a transmitted beam and reflected beam by a 50%-50% beam splitter, then detected by two detectors, separately; and finally the correlation between the two detectors is calculated.

Fig. 4 shows two examples of the second-order quantum correlation function using an ideal single photon source. The single emitter, excited with a continuous wave source (see Fig. 4a), has a $g^{(2)}(\tau = 0)$ that is equal to exactly zero, because there is only one photon at a time. We can understand this behaviour as follows: the single photon emitter "selects" a photon, which is coherent in its own way, out of the beam, then emits it into a desired mode; thus, the emitted photon only depends upon the properties of the single photon emitter. After this operation, one obtains a single photon source with no noise. The other example, shown in Fig. 4b, is excited by a train of optical pulses. In this latter case, each pump pulse will give rise to the emission of a single photon; the correlation function of the pulsed pumping scheme is a Dirac comb of short peaks, but with the zero-time peak missing; because only one photon is produced, there can be no coincidences between the two detectors for zero delay. The examples shown are *ideal*, and we remark that typically there are rich features near the region of zero delay, that depend on the precise details of the radiative and nonradiative decay channels, as well as pure dephasing processes in the solid state environment.

## 3. Exact quantum field operator and the Purcell effect for a QD in an arbitrary inhomogeneous dielectric

As we have alluded in the introduction, there are three essential criteria for producing practical single-photon sources: *i*) sufficient suppression of the effects of decoherence or pure dephasing during the photon emission process; *ii*) efficient excitation of the photon emitter (QD); and *iii*) efficient extraction and thus manipulation of the emitted photons. The first criterion can be achieved by placing the QDs in an environment that increases the local photon density of states (LDOS) through the Purcell effect. The Purcell factor is a measure of the vacuum-induced spontaneous emission rate enhancement, defined by $\Gamma/\Gamma_0$, where $\Gamma$ (the *Einstein A coefficient*) is the spontaneous emission rate associated with population decay rate from an excited state to the ground state, and $\Gamma_0$ is the spontaneous emission rate in a homogeneous medium with some nominal background refractive index.

The classical electrodynamical properties can be obtained from Maxwell's equations. To describe the general theory of light emission, we first define the photon Green function and the eigenmodes of the system. The two-space point function $\mathbf{G}(\mathbf{r}, \mathbf{r}'; \omega)$ is the electric-field Green function that describes the field response at $\mathbf{r}$ to an oscillating polarization dipole (source) at $\mathbf{r}'$, as a function of frequency; the Green function is classical and is defined from

$$\left[\nabla \times \nabla \times -\frac{\omega^2}{c^2}\varepsilon(\mathbf{r})\right] \mathbf{G}(\mathbf{r}, \mathbf{r}', \omega) = \frac{\omega^2}{c^2}\mathbf{1}\delta(\mathbf{r} - \mathbf{r}'), \quad (3)$$

where $\mathbf{1}$ is the unit dyadic. The Green function $\mathbf{G} = \mathbf{G}^{\mathrm{T}} + \mathbf{G}^{\mathrm{L}}$, contains contributions from both transverse and longitudinal modes, and can be written as $\mathbf{G}(\mathbf{r}, \mathbf{r}'; \omega) = \sum_\lambda \{\omega^2 \mathbf{f}_\lambda^{\mathrm{T}}(\mathbf{r})[\mathbf{f}_\lambda^{\mathrm{T}}(\mathbf{r}')]^*/(\omega_\lambda^2 - \omega^2) - \mathbf{f}_\lambda^{\mathrm{L}}(\mathbf{r})[\mathbf{f}_\lambda^{\mathrm{L}}(\mathbf{r}')]^*\}$, where $\mathbf{f}_\lambda^{\mathrm{T/L}}$ are the generalized transverse and longitudinal modes of the medium corresponding to $\nabla \cdot \mathbf{D} = 0$ and $\nabla \cdot \mathbf{D} \neq 0$, respectively, where $\mathbf{D}$ is electric displacement field. The transverse modes, $\mathbf{f}_\lambda^{\mathrm{T}} \equiv \mathbf{f}_\lambda$, are solutions of non-zero eigenvalue: $\left[\boldsymbol{\nabla} \times \boldsymbol{\nabla} \times -\omega_\lambda^2/c^2\,\varepsilon(\mathbf{r})\right] \mathbf{f}_\lambda(\mathbf{r}) = 0$. These modes are easily computed for most cavities and PC media using standard electromagnetic techniques, and one can also frequently compute the numerically-exact Green function. Another useful Green function is defined through [38] $\mathbf{K}(\mathbf{r}, \mathbf{r}'; \omega) = \sum_\lambda \omega_\lambda^2 \mathbf{f}_\lambda(\mathbf{r})[\mathbf{f}_\lambda(\mathbf{r}')]^*/(\omega_\lambda^2 - \omega^2)$, which, like $\mathbf{G}^{\mathrm{T}}$, only depends on the transverse modes of the system. Note that we have exploited the relation, $\mathbf{1}\delta(\mathbf{r} - \mathbf{r}') = \sum_\lambda [\mathbf{f}_\lambda(\mathbf{r})\mathbf{f}_\lambda^*(\mathbf{r}')\varepsilon(\mathbf{r}) + \mathbf{f}_\lambda^{\mathrm{L}}(\mathbf{r})(\mathbf{f}_\lambda^{\mathrm{L}})^*(\mathbf{r}')\varepsilon(\mathbf{r})]$. The following

relationships can also be derived: $\mathbf{K} = \mathbf{G}+\mathbf{1}\delta(\mathbf{r}-\mathbf{r}')/\varepsilon(\mathbf{r})$, and $\mathbf{K} = \mathbf{G}^{\mathrm{T}} + \boldsymbol{\delta}^{\mathrm{T}}(\mathbf{r},\mathbf{r}')/\varepsilon(\mathbf{r})$, where $\boldsymbol{\delta}^{\mathrm{T}}(\mathbf{r},\mathbf{r}') = \sum_\lambda \mathbf{f}_\lambda(\mathbf{r})\mathbf{f}_\lambda^*(\mathbf{r}')\varepsilon(\mathbf{r})$ is a generalized transverse delta function [38].

Next, we introduce some of the basic quantum mechanics. To describe quantized light emission in an arbitrary inhomogeneous dielectric, we employ a canonical Hamiltonian of the form [38,39] (the time dependence is implicit):

$$\hat{H} = \hbar\omega_x\hat{\sigma}_x^+\hat{\sigma}_x^- + \sum_\lambda \hbar\omega_\lambda\hat{a}_\lambda^\dagger\hat{a}_\lambda - i\hbar\sum_\lambda\left(\hat{\sigma}_x^- + \hat{\sigma}_x^+\right)\left(g_\lambda\hat{a}_\lambda - g_\lambda^*\hat{a}_\lambda^\dagger\right), \quad (4)$$

where $\hat{a}_\lambda$ represents the field mode operators, $\hat{\sigma}_x^{+/-}$ are the Pauli operators of the QD excitons (where we assume one QD exciton in the frequency regime of interest), and the QD-photon interaction terms are treated within the dipole approximation (valid for photon emitters whose spatial size is much smaller than a wavelength); in addition, $\omega_x$ is the resonant frequency of the QD, $\omega_\lambda$ is the eigenfrequency corresponding to the transverse modes of the system ($\mathbf{f}_\lambda(\mathbf{r})$) *excluding* the dots; and $g_\lambda$ is the field-dot coupling coefficient: $g_\lambda = \sqrt{\frac{\omega_\lambda}{2\hbar\varepsilon_0}}\boldsymbol{\mu}\cdot\mathbf{f}_\lambda(\mathbf{r}_d)$, where $\boldsymbol{\mu} = \mathbf{n}_d\mu$ is the optical dipole moment of the QD electron-hole pair, and $\mathbf{n}_d$ is the dipole unit vector; the QD is at the spatial position $\mathbf{r}_d$. The Heisenberg equations of motion for the operators can be derived from $\dot{\hat{O}}_i = -i\hbar^{-1}[\hat{O}_i, H]$, yielding

$$\frac{d\hat{a}_\lambda}{dt} = -i\omega_\lambda\hat{a}_\lambda + g_\lambda^*\left(\hat{\sigma}_x^- + \hat{\sigma}_x^+\right), \quad (5)$$

$$\frac{d\hat{a}_\lambda^\dagger}{dt} = i\omega_\lambda\hat{a}_\lambda^\dagger + g_\lambda\left(\hat{\sigma}_x^- + \hat{\sigma}_x^+\right), \quad (6)$$

$$\frac{d\hat{\sigma}_x^-}{dt} = -i\omega_x\hat{\sigma}_x^- - \sum_\lambda\left(g_\lambda\hat{a}_\lambda - g_\lambda^*\hat{a}_\lambda^\dagger\right), \quad (7)$$

$$\frac{d\hat{\sigma}_x^+}{dt} = i\omega_x\hat{\sigma}_x^+ + \sum_\lambda\left(g_\lambda\hat{a}_\lambda - g_\lambda^*\hat{a}_\lambda^\dagger\right). \quad (8)$$

Subsequently, one can perform a Laplace transformation of the above equation set, and relate to the formal definition of the electric-field operator: $\hat{\mathbf{E}}(\mathbf{r},t) = i\sum_\lambda\sqrt{\frac{\hbar\omega_\lambda}{2\varepsilon_0}}\hat{a}_\lambda(t)\mathbf{f}_\lambda(\mathbf{r}) + \mathrm{H.c.}$. As an example, assuming a QD exciton, with the field in vacuum, one can derive the *exact* electric field operator:

$$\hat{\mathbf{E}}(\mathbf{r},\omega) = \frac{\mathbf{K}(\mathbf{r},\mathbf{r}_d;\omega)\cdot\hat{\mathbf{d}}}{1-\mathbf{n}_d\cdot\mathbf{K}(\mathbf{r}_d,\mathbf{r}_d,\omega)\cdot\mathbf{n}_d\,\alpha_0(\omega)}, \quad (9)$$

where we introduce the bare polarizability, $\alpha_0(\omega) = 2\omega_x\mu^2/[(\hbar\varepsilon_0)(\omega_x^2-\omega^2)]$, and a quantum dipole source

$$\hat{\mathbf{d}}(\omega) = \frac{i\boldsymbol{\mu}}{\varepsilon_0}\left(\frac{\hat{\sigma}_x^-(t=0)}{\omega-\omega_x} + \frac{\hat{\sigma}_x^+(t=0)}{\omega+\omega_x}\right). \quad (10)$$

The interpretation of the above quantum dipole is similar to what occurs classically, where the bare polarizability is medium-dressed or renormalized by the surrounding medium, which then properly accounts for radiative coupling to the photon modes. The subtle difference between the quantum and classical fields, is that in the quantum case, the dipole source above stems from quantum noise or vacuum fluctuations, and the Green function $\mathbf{K}$ appears, rather than $\mathbf{G}$ [38]. We can rearrange the quantum field operator to better connect to the more familiar self-energy term, $\Sigma(\omega)$:

$$\hat{\mathbf{E}}(\mathbf{r},\omega) = \frac{i\mathbf{K}(\mathbf{r},\mathbf{r}_d;\omega)\cdot\boldsymbol{\mu}}{\varepsilon_0} \times \frac{[\hat{\sigma}_x^-(t=0)(\omega+\omega_x) + \hat{\sigma}_x^+(t=0)(\omega-\omega_x)]}{\omega_x^2-\omega-\omega\Sigma(\omega)}, \quad (11)$$

where

$$\omega\Sigma(\omega) = \frac{2\mu^2\omega_x}{\hbar\varepsilon_0}\mathbf{n}_d\cdot\mathbf{K}(\mathbf{r}_d,\mathbf{r}_d;\omega)\cdot\mathbf{n}_d\,. \quad (12)$$

The imaginary part of the self-energy defines the spontaneous emission rate

$$\begin{aligned}\Gamma(\mathbf{r}_d,\omega) &= \frac{2\mu^2\,\mathbf{n}_d\cdot\mathrm{Im}[\mathbf{K}(\mathbf{r}_d,\mathbf{r}_d;\omega)]\cdot\mathbf{n}_d}{\hbar\varepsilon_0} \\ &= \frac{2\mu^2\,\mathbf{n}_d\cdot\mathrm{Im}[\mathbf{G}(\mathbf{r}_d,\mathbf{r}_d;\omega)]\cdot\mathbf{n}_d}{\hbar\varepsilon_0} \\ &= \frac{2\mu^2\,\mathbf{n}_d\cdot\mathrm{Im}[\mathbf{G}^{\mathrm{T}}(\mathbf{r}_d,\mathbf{r}_d;\omega)]\cdot\mathbf{n}_d}{\hbar\varepsilon_0}, \end{aligned} \quad (13)$$

which would be the decay rate of the population from an upper excited state to ground, with an initial quantized field in vacuum; therefore, the process of spontaneous emission can be thought of as stimulated emission from the vacuum, and thus both spontaneous and stimulated emission have the same quantum mechanical origin. For obtaining the spontaneous emission rate, evidently one can work with $\mathbf{K}$, $\mathbf{G}$, or $\mathbf{G}^{\mathrm{T}}$ above. Note also that the terminology of spontaneous emission "rate" only makes sense for a weak or intermediate coupling regime. We stress, however, that the general formalism above rigorously covers both weak and strong coupling regimes in a self-consistent way, naturally recovering phenomena such as vacuum Rabi oscillations and reverse spontaneous emission [40–42]. Our expression for the spontaneous emission is also in agreement with derivations from Dung et al. [43,44] and Wubs et al. [38], who have pioneered many of the general theories of quantized light emission within inhomogeneous materials. In a similar manner, one can also obtain a frequency shift of the QD exciton, defined through $\Delta\omega = \mu^2\,\mathbf{n}_d\cdot\mathrm{Re}[\mathbf{K}(\mathbf{r}_d,\mathbf{r}_d;\omega)]\cdot\mathbf{n}_d/\hbar\varepsilon_0$. This contribution includes an electronic vacuum Lamb shift [45], as well as the inhomogeneous *photonic* contribution, which would typically be the dominant and measurable contribution. Since computation of the vacuum Lamb shift requires a careful mass renormalization formalism, it is more convenient and practical to compute the photonic contribution

from the inhomogeneous structure, and subtract off the homogeneous contribution.

We next introduce some convenient approximations for a planar PC medium, in which a well defined transverse mode is the dominant contribution. Since $\mathbf{G}^{\mathrm{T}}(\mathbf{r},\mathbf{r}';\omega) = \mathbf{K}(\mathbf{r},\mathbf{r}';\omega) - \boldsymbol{\delta}^{\mathrm{T}}(\mathbf{r},\mathbf{r}')/\varepsilon(\mathbf{r})$, then $\mathbf{G}^{\mathrm{T}}_m \approx \mathbf{K}_m$, where $m$ represents the dominant modal contribution to the Green function; e.g., $m = c$ or $m = w$ could be the cavity or waveguide mode Green function that dominates as it appears within a photonic bandgap. This allows us to write out the *dominant modal contribution* to the decay rate and frequency shift, respectively, as

$$\Gamma(\mathbf{r}_d,\omega) \approx \frac{2\mu^2\,\mathbf{n}_d\cdot\mathrm{Im}[\mathbf{G}^{\mathrm{T}}_m(\mathbf{r}_d,\mathbf{r}_d;\omega)]\cdot\mathbf{n}_d}{\hbar\varepsilon_0} \qquad (14)$$

and

$$\Delta\omega(\mathbf{r}_d,\omega) \approx \frac{\mu^2\,\mathbf{n}_d\cdot\mathrm{Re}[\mathbf{G}^{\mathrm{T}}_m(\mathbf{r}_d,\mathbf{r}_d;\omega)]\cdot\mathbf{n}_d}{\hbar\varepsilon_0}\,. \qquad (15)$$

Finally, we obtain a formal expression for the Purcell effect factor:

$$F(\mathbf{r}_d,\omega) = \frac{\mathbf{n}_d\cdot\mathrm{Im}[\mathbf{G}^{\mathrm{T}}_m(\mathbf{r}_d,\mathbf{r}_d;\omega)]\cdot\mathbf{n}_d}{\mathbf{n}_d\cdot\mathrm{Im}[\mathbf{G}^{\mathrm{T}}_{\mathrm{hom}}(\omega)]\cdot\mathbf{n}_d}\,, \qquad (16)$$

where $\mathbf{n}_d\cdot\mathrm{Im}[\mathbf{G}^{\mathrm{T}}_{\mathrm{hom}}(\omega)]\cdot\mathbf{n}_d = \omega^3\sqrt{\varepsilon_b}/(6\pi c^3)$, with $\varepsilon_b$ the dielectric constant of a homogeneous material.

## 4. Single photon emission within a PC cavity

Advanced lithography and etching techniques have recently led to major improvements in the fabrication of nanoscale PCs; most notably has been the spectacular increase in the quality factor ($Q$) and decrease in effective mode volume ($V_{\mathrm{eff}}$) of planar PC nanocavities [46]. These nanoscale cavities are enabling the study of fundamentally new regimes of light-matter interaction, such as single-exciton QED [47]. Therefore, the most common PC structure to date for trying to demonstrate a single photon source is the PC cavity [48–50].

A simple PC cavity can be realized by adding a defect into the perfect PC slab, for example, by removing one hole. Moreover, it has been demonstrated, through new design insights, that very large $Q/V_{\mathrm{eff}}$ values can be realized. In Fig. 5, we show the popular L3 cavity [46], based on the design of Akahane et al. [46]. The physics of this cavity mode is well established: light is trapped by the high-index-contrast PC in the $x$- and $y$-directions, and bound as much as possible by total internal reflection in the $z$-direction. Coupling of the field mode to radiation modes above the light line causes decay of the field within the cavity; this coupling is minimized by moving two of the holes [46], resulting in a large $Q$. These large $Q/V_{\mathrm{eff}}$-cavities were first demonstrated for silicon membranes, but recent experiments on InP [51] and GaAs [52] cavities, show that the fabrication quality with these III-V materials is becoming comparable with silicon.

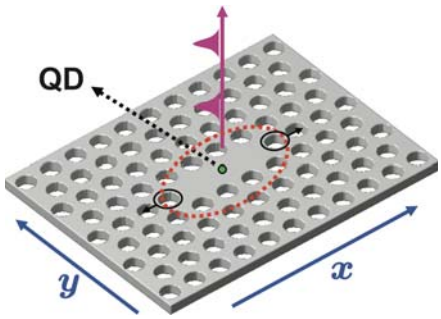


**Figure 5** (online color at: www.lpr-journal.org) Schematic diagram of single photon source based on a monolithic cavity; the green dot refers to the quantum dot, and the photon is emitted vertically via the leaky cavity mode. The highlighted holes with the black circles are the holes that can be shifted (outwards along $x$) from the nominal lattice position to improve the $Q$ of the cavity.

To maximize the Purcell effect, one needs to have the QD spatially positioned near the antinode of the localized cavity mode field. Using randomly arranged self-assembled QDs, 30 nm accuracy can be achieved by strategically monitoring the QD position via atomic force microscopy (AFM) technology [50]. In this way, QDs within the center of the slab membrane may be located, prior to writing the PC with e-beam lithography. Certainly, a major on-going challenge that needs to be addressed, experimentally, is how to place the QDs in the position of interest, in a more *deterministic* manner, but progress is being made.

The spontaneous emission of the target QD exciton will be enhanced if it is coupled to the cavity mode, both spatially and spectrally; for an uncoupled QD, the emission will be inhibited due to the presence of the slab and the photonic bandgap. Assuming that the microcavity supports a single cavity mode, the transverse Green function of the monolithic cavity can be expressed as $\mathbf{G}^{\mathrm{T}}_c(\mathbf{r},\mathbf{r}';\omega) = \omega^2\mathbf{f}_c(\mathbf{r})\mathbf{f}^*_c(\mathbf{r}')/(\omega_c^2 - \omega^2 - i\omega\Gamma_0)$, where $\omega_c$ is the resonance frequency of the cavity mode, which is deep inside the photonic bandgap; in addition, $\mathbf{f}_c(\mathbf{r})$ is the localized eigenmode normalized through $\int d\mathbf{r}\varepsilon_c(\mathbf{r})\mathbf{f}_c(\mathbf{r})\mathbf{f}^*_c(\mathbf{r}) = 1$, and $\Gamma_0 = \omega_c/Q$ is the cavity linewidth rate. Another useful cavity parameter is the effective mode volume, which can be defined from the cavity eigenmode $\mathbf{f}_c(\mathbf{r})$: $V_{\mathrm{eff}} = 1/\max[\varepsilon_c(\mathbf{r})\mathbf{f}_c(\mathbf{r})\mathbf{f}^*_c(\mathbf{r})]$. It should be noted that this expression is only approximately true for leaky modes. Thus, using the earlier results of the theory section, the enhancement of spontaneous emission for a QD resonant with a cavity mode can be expressed as

$$F = 6\pi\frac{AQ}{V_{\mathrm{eff}}}\left(\frac{c}{\sqrt{\varepsilon_c}\,\omega}\right)^3\,, \qquad (17)$$

where $A$ is a coupling constant related to the deviation of the QD from the antinode (i.e., $A = 1$ if the QD is precisely placed at the field antinode).

From the above approximate formulas, and using physically intuitive parameters such as the $Q$ factor and the

local electric field at the field antinode, we can obtain some qualitative results for the Purcell factor. Further rigorous calculations of the spontaneous emission can be calculated by carrying out a direct numerical computation of the photon Green function [53], by solving the Maxwell equations, excited by a polarization dipole source. To do this, for example, one can use FDTD (finite-difference time domain) techniques [54][1]. In FDTD, the electric field is excited by a dipole source $\mathbf{p}$, which satisfies

$$\left[\nabla \times \frac{1}{\mu(\omega,\mathbf{r})}\nabla \times -\frac{\omega^2}{c^2}\varepsilon(\omega,\mathbf{r})\right]\mathbf{E}(\mathbf{r},\omega) = \frac{\omega^2}{c^2}\mathbf{p}(\omega)\delta(\mathbf{r}-\mathbf{r}'), \quad (18)$$

where $\varepsilon(\omega,\mathbf{r})$ ($\mu(\omega,\mathbf{r})$) is the frequency-dependent permittivity (permeability). Subsequently, the $ii$-th component of the numerical Green function is

$$G_{ii}(\mathbf{r},\mathbf{r}_s;\omega) = \frac{\mathrm{FFT}[E_i^m(\mathbf{r},t)]}{\mathrm{FFT}[p_i^s(\mathbf{r}_s,t)]} = \frac{E_i^m(\mathbf{r},\omega)}{p_i^s(\mathbf{r}_s,\omega)}, \quad (19)$$

where FFT is a Fourier transform of the numerical fields obtained by FDTD. The precise accuracy is dependent on the grid size in the simulation volume; however, for sufficiently small spatial grids, the results are found to be very accurate. For example, using a grid size that is 1/25 of the central wavelength $\lambda_0$ of the incident pulse, we have checked against known analytical solutions that the error is less than 1% over a broadband frequency range of 0.5–1.3 $(2\pi c/\lambda_0)$.

We first investigate the case of a single photon source based on a L3 PC cavity shown in Fig. 5. The structural parameters used in this simulation are as follows: semiconductor slab index $n = 3.464$, lattice constant $a = 420$ nm (PC pitch), two-hole outward shift length of $0.15\,a$, slab thickness and hole radius are $0.5\,a$ and $0.275\,a$, respectively. The TE-like band-gap ranges from 185 to 228 THz – or 0.26–0.32 $c/a$ in scaled frequency units.

In Fig. 6, we show the Purcell factor for a perfectly positioned and aligned QD (maximum coupling), which is calculated directly by the 3D FDTD simulation. Therefore, we are actually showing the "exact" Purcell factor (at least in the absence of strong coupling). The Purcell factor for the $y$-polarized exciton is as high as $F_y = 3385$ at the resonant frequency of 192.78 THz. We emphasize that the theoretical maximum Purcell factor of 3385 is the *ideal* enhancement rate of spontaneous emission, because several ideal conditions are assumed, for example, the QD is maximally coupled to the antinode of the cavity mode and perfectly resonant with the cavity mode frequency. The concept of a spontaneous emission rate – as a measure of spontaneous emission – only make sense for weak to intermediate coupling regimes, which depends upon the dipole moment of the emitter as well as the material coupling parameters.

[1] We use FDTD Solutions, by Lumerical Solutions Inc., as well as some of our own in-house FDTD codes.

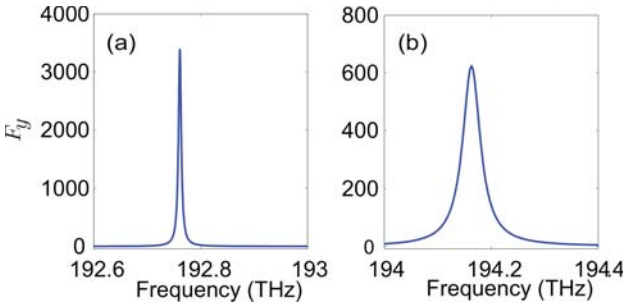


**Figure 6** (online color at: www.lpr-journal.org) Theoretical maximum Purcell factors ($F_y$) versus frequency for a QD embedded in a shifted-hole cavity (a) and a no-shift cavity (b). In practise, such a well-coupled QD exciton would already be in the regime of strong coupling, so one can think of these as enhancements of the projected LDOS.

For typical self-assembled QDs, assuming maximum coupling as above, then we would already be in the strong coupling regime. Therefore, in general one can think of the Purcell factor here as representing the properties of the dielectric environment *without* a self-consistent coupling to the emitter, i.e. the LDOS or the projected LDOS. We stress, however, that the above Green function theory can be used to study weak to strong coupling regimes without any change in formalism [55, 56]. In reality, sample imperfections and finite material loss will also reduce this estimated maximum value, as discussed in more detail below.

For this peak enhancement frequency, the corresponding electric-field distribution of the $y$-polarized resonant mode, at the center of the slab, is shown in Fig. 7. The quality factor and the effective volume are 31 432 and 0.0627μm$^3$, respectively. With these parameters, the approximate Purcell factor can also be calculated from Eq. (17), which yields 3981, and is notably *larger* than 3385. Therefore, the usual formula for the Purcell factor (Eq. (17)) can only be used as an approximation; the origin of this discrepancy is that the confined mode is a quasi-mode or leaky-mode, where the mode can leak out over larger volumes that what would be estimated in a finite-size numerical calculation. In most realistic devices, the spatial positions of the QDs will always deviate from the electric-field maximum; for example, if located at 90% of the peak electric field, then the Purcell factor enhancement will be reduced to about 80% of its peak value; in addition, the enhancement also suffers from fabrication imperfections, that can partly reduce the quality factor [57, 58] and can also cause

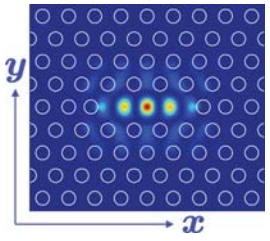


**Figure 7** (online color at: www.lpr-journal.org) The spatial distribution of the electric field amplitude, corresponding to the peak Purcell factor in Fig. 6a.

a shift in the resonance of the cavity mode [59, 60]. For comparison, we also calculate the emission properties of the no-shift cavity (see Fig. 6b), which gives a much smaller Purcell factor of only 624, and a quality factor of 4856.

For experiments in the intermediate-to-strong-coupling regime, with self-assembled QDs, Hennessy et al. [50] investigated the quantum nature of a QD embedded in a similar PC cavity to that shown above. For a large off-resonant case, with a detuning of $4.1$ nm (5.7 meV), the exciton lifetime $\tau_x$ is increased to $8.7$ ns from 1 ns (the exciton lifetime in a bulk material). While for the resonant case ($\omega_x \approx \omega_c$), $\tau_x$ *decreases rapidly* to only $60$ ps, which is only about $\frac{1}{134}$ of the off-resonant value. This certainly confirms that pronounced Purcell effects can be realized. A related theory of the spectral observations and second-order quantum correlation measurements are presented elsewhere [56, 61] (see also [62–64]), which in general show the need for a medium-dependent theory, namely a theory that is based on quantizing the medium-dependent macroscopic electric field operators; using such a quantization procedure, the relationship between the electric field operators and the exciton operators is established directly with the medium-based Green functions; this helps to clarify the underlying physics of photon emission processes in these chip-based structures, since unexpected observations can occur such as off-resonance excitation of the cavity mode [50, 56].

## 5. Single photon source using PC waveguides

### *5.1. The infinite-size PC waveguide: open system cavity-QED*

One major drawback of using the monolithic quasi closed-cavity is that the photons vertically emitted out of the cavity cannot be efficiently collected and manipulated. Moreover, it is against the general vision of *planar integration*, and one ultimately desires to emit the photon on-chip, into a target propagating mode. This is exactly where the unique advances of planar PCs come in; compared to other microcavity systems such as the micropillars and microdisks, PC waveguides have the inherent advantage that they can collect and control the photons on-chip [65–68]. In fact, enhanced spontaneous emission does not even need a quasi-closed cavity such as that shown with the L3 cavity, and *open system cavity-QED* can be exploited to achieve an LDOS enhancement by appropriate bandgap engineering of the propagation modes.

Kleppner predicted in 1981 [69], that photon emission rates can be enhanced using cylindrical metallic-wire waveguides, for emission frequencies lying near the mode bandedge. Although these modes are usually lossy, the idea introduced the general concept that single photon emission into a photonic wire is both rich in physics and applications. The photonic wire, such as a bar of silicon surrounded by air, uses the high-index-contrast to confine light at selected wavelengths, using the principle of total internal reflection. By embedding a photon emitter at the center of such a photonic wire [70], significant collection efficiencies can be achieved: $\sim 50$–$80\%$ into a bound propagation mode, however, there is very little spontaneous emission enhancement which is necessary for solid-state single photon emission applications to overcome the known problems of decoherence. The relationship between slow-light modes and spontaneous enhancement can be obtained from the Green function of the PC waveguide structure [71], and is discussed in some detail below.

We first assume an ideal structure (no disorder or finite-size effects), described through the spatially-dependent dielectric constant $\varepsilon_w(\mathbf{r})$, as schematically illustrated in Fig. 8a; and although this only shows eight unit cells along the waveguide axis, keep in mind that we modeling an infinite structure (in the $x$-direction). The structure supports a Bloch waveguide mode (cf. the solid curve in the band structure plot), which, in the region below the light line, is lossless in the absence of disorder; the ideal group velocity is then $v_g = \mathrm{d}\omega/\mathrm{d}k$. The physics of PC waveguides is rather intriguing, with the defining feature that their engineered waveguide band dispersions yield a vanishing group velocity [72–74].

In Fig. 8b we show an example of the planar PC waveguide band structure, which displays the two lowest order propagation modes. For PC propagation modes below the

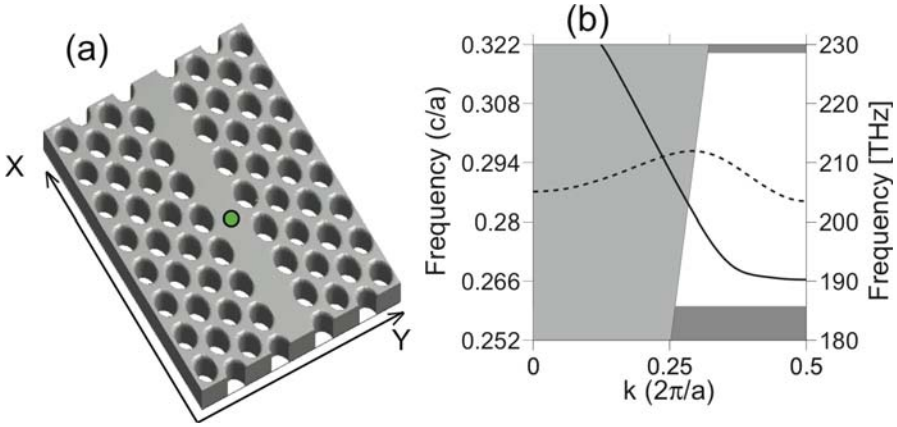


**Figure 8** (online color at: www.lpr-journal.org) (a) Schematic of a planar PC waveguide (W1) along the $x$-axis and a single quantum dot (QD: filled green circle) embedded at the center of the slab. (b) The band structure of modes (solid/dashed curves) corresponding to an infinite length planar PC waveguide (PC parameters as in Figure 5) shown within the TE-like band-gap. The grey shaded region above the light line represents the continuum of radiation modes.

light line, described by $\mathbf{f}_k(\mathbf{r}) = \sqrt{\frac{a}{L}}\mathbf{e}_k(\mathbf{r})e^{ikx}$, the waveguide Green function can be expressed as

$$\mathbf{G}_w^{\mathrm{T}}(\mathbf{r},\mathbf{r}';\omega) = \sum_k \frac{\omega^2}{\omega_k^2-\omega^2}\mathbf{f}_k(\mathbf{r})\mathbf{f}_k^*(\mathbf{r}')\,. \tag{20}$$

Replacing the $k$-summation ($k \equiv k_x$) by an integral, i.e., $\sum_k \rightarrow \frac{L}{2\pi}\int dk$, where $L$ is the length of the waveguide,

$$\mathbf{G}_w^{\mathrm{T}}(\mathbf{r},\mathbf{r}';\omega) = \frac{L}{4\pi}\int_{-\infty}^{\infty} dk \frac{\omega}{\omega_k-\omega-i\delta}\mathbf{f}_k(\mathbf{r})\mathbf{f}_k^*(\mathbf{r}')\,, \tag{21}$$

with $\delta$ a positive infinitesimal variable. After carrying out the complex pole integration,

$$\begin{aligned}&\mathbf{G}_w^{\mathrm{T}}(\mathbf{r},\mathbf{r}';\omega)\\ &= \frac{ia\omega}{2v_g}\Big[\Theta(x-x')\mathbf{e}_{k_\omega}(\mathbf{r})\mathbf{e}_{k_\omega}^*(\mathbf{r}')e^{ik_\omega(x-x')}\\ &\qquad + \Theta(x'-x)\mathbf{e}_{k_\omega}^*(\mathbf{r})\mathbf{e}_{k_\omega}(\mathbf{r}')e^{-ik_\omega(x-x')}\Big]\,,\end{aligned} \tag{22}$$

where we treat $v_g$ as positive, and $\Theta(x-x')$ is the Heaviside function. Note also that $\mathrm{K}_w = \mathrm{G}_w^{\mathrm{T}}$ above, because of the continuum nature of the waveguide modes ($\omega_k = \omega$); so one can work with either function. Since the Purcell factor ($\propto \mathrm{Im}[G]$) is inversely proportional to the group velocity $v_g$, slow light modes will exhibit pronounced enhanced emission [71]; and with typically significantly more bandwidth than that might be achieved by using nanowband defect cavity modes.

Interestingly, the Purcell factor tends towards infinity at the waveguide band edge. However, this divergence never happens in real structures primarily because of fabrication imperfections; this is not necessarily a disaster, since there are certainly ways to make useful devices once one understands and accounts for imperfections as well. For example, Hughes et al. [75] introduced a PC wave-guide model for *incoherent* extrinsic scattering in the slow-light regime. With $v_g$ the group velocity, they predicted that the *ensemble average* backscattering loss, for weak perturbative disorder, scales as $1/v_g^2$ and dominates over scattering into radiation loss modes ($1/v_g$ scaling). Similar scalings have been found by Povinelli et al. [76] and by Gerace and Andreani [77]. These general approximate loss-scaling relations have now been confirmed experimentally by a number of groups, e.g. [78–80], except that they naturally break down at extremely low group velocities where using the ideal band structure is no longer a good approximation [81]. In this case, the effective group velocity will be noticeably altered from the ideal value for around $v_g \lesssim c/35$, and will have a minimum of around $c/50 - c/200$; related effects also occur in coupled-cavity structures using PC cavities [59], and we refer the interested reader to the works of, for example, Fussell et al. [59], Engelen et al. [80], and Patterson et al. [82]. For the present purpose, we note that fabrication disorder introduces a minimum achievable group velocity and thus a maximum Purcell effect, and the nominal lossless waveguide modes become very lossy in the regime of slow light (where multiple scattering effects begin to dominate [82]). This suggests that long waveguides, operating in the slow light regime, will be impractical for single photon applications; we will come back to this point later.

A key design parameter for efficient photon extraction of a single photon is the *single photon $\beta$ factor*, which is related to the collection efficiency of the output photon into a desired mode. The $\beta$ factor was traditionally proposed in order to quantify the lasing efficiency from spontaneous emission into a desired lasing mode. Here, we define the single-photon $\beta$ factor as the fraction of the emitted light that goes into a target waveguide mode, i.e. the probability of a photon being emitted into a waveguide mode. Neglecting the possible impact of extrinsic scattering losses (but keeping in mind the minimum group velocity), the $\beta$ factor for a planar PC waveguide can be written as [83]:

$$\beta = \frac{\Gamma_{\mathrm{bound}}}{\Gamma_{\mathrm{bound}}+\Gamma_{\mathrm{rad}}+\Gamma_{\mathrm{nr}}}\,, \tag{23}$$

where $\Gamma_{\mathrm{bound}}$ is the decay rate into the target bound waveguide mode, $\Gamma_{\mathrm{rad}}$ is related to the decay of the spontaneous emission into a radiation modes (modes above the light line), and $\Gamma_{\mathrm{nr}}$ is the nonradiative decay rate due to various dephasing processes. For low temperatures of around 4 K, the non-radiative relaxations typically occur on a much longer time scale than radiative transitions (especially in an enhanced emission regime). Therefore, the $\beta$ factor can be simplified to $\beta = \Gamma_{\mathrm{bound}}/(\Gamma_{\mathrm{bound}}+\Gamma_{\mathrm{rad}})$, which is valid for low temperature operation.

Recently we have presented an analytical Green-function formalism to calculate the Purcell factor and the $\beta$ factor of an ideal planar PC waveguide [83], which extends earlier work on the Purcell factor alone [71]. Using the structure depicted in Fig. 8, we show in Fig. 9a an example of the electric-field distribution of guided mode $\mathbf{f}_y$-component with a slow group velocity (at $k_\omega = 0.47\,(2\pi/a)$, with $v_g \sim c/154$) for one unit-cell of the waveguide, where most of the energy is localized within the center of the slab. This wave vector was chosen as a typical upper $k$ limit (smaller group velocity) that can be measured experimentally [84, 85]. The corresponding effective mode volume (per unit cell [83]) is only $V_{\mathrm{eff}} = 0.03\,\mu\mathrm{m}^3$. The mode-volumes of the broadband waveguide modes range from 0.02–0.03 $\mu\mathrm{m}^3$, which correspond to $k$ values of 0.3–0.48 $(2\pi/a)$. An example *spatial map* of the Purcell factor for a $y$-polarized dipole (see Fig. 9b) is also presented as a function of QD position, on a plane parallel to the slab for $k_\omega = 0.47\,(2\pi/a)$. Substantial enhancements in the spontaneous emission rate by up to a factor of 30 are achievable, which will become even greater for smaller group velocities. As can be seen, if the same dipole was placed away from the anti-node position, the Purcell factor would reduce substantially as it scales with the field strength squared. Hence there is a "hot spot" area of around $\pi(80\,\mathrm{nm})^2$ that yield

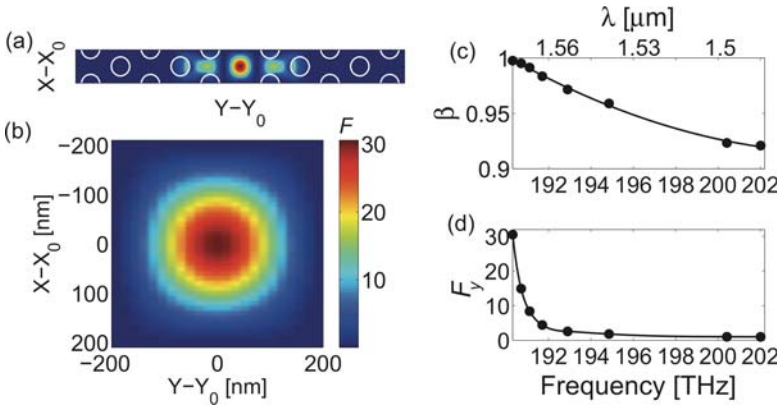


**Figure 9** (online color at: www.lpr-journal.org) (a) Example electric field profile of the $y$-component ($|\mathbf{f}_y(\mathbf{r})|^2$) of a slow-light mode on the plane parallel to the slab, and located at mid-plane of the slab ($z = 0$); the wavevector is $k = 0.47\,(2\pi/a)$ and the corresponding group-index $n_g = 154$. The superimposed white circles show boundaries of air-holes in the slab. (b) Purcell factor ($F_y$) as a function of QD position on the same plane as in (a) for a slow-light mode with dipole orientation along the $y$-axis. (c) $\beta$ factor as a function of fundamental mode frequency for the case of a $y$-oriented dipole, positioned at the field anti-node. (d) The corresponding Purcell factor.

Purcell factors of greater than 20. The peak Purcell factors and $\beta$ factors as a function of frequency are shown in Fig. 9c,d. Most remarkably, is the fact that enhanced $\beta$ factors ($> 0.9$) can be maintained with a substantial bandwidth ($> 10$ THz or 60 nm), which is in stark contrast to the usual cavity-QED regimes that exploit narrowband cavities. Similar findings were reported by Lecamp et al. [86], who also exploited periodic Bloch mode analysis. Related studies by Fussell et al. investigated the strong coupling regime between a QD and a lossy coupled-cavity waveguide by the tight-binding approach [87]; however, later investigation in the present of fabrication disorder [59], concluded that strong coupling effects would likely be destroyed because of a significant broadening of the LDOS at the waveguide bandedge.

With regards to these theoretical predictions, some related experiments have been performed. In 2005, Viasnoff-Schwoob et al. [88] presented evidence for the spontaneous emission enhancement of QD exciton decay coupled to a leaky mode in a planar PC waveguide, using out-of-plane and in-plane light emission measurements. More recent experiments on bound waveguide modes below the light line have been carried out by Lund-Hansen et al. [89], who observe enhanced emission in the slow-light regime, and find good agreement with our analytical formulas presented above. Specifically, Lund-Hansen et al. performed time-resolved spontaneous emission measurements on single QD positioned within the planar PC waveguide, where the QDs are excited by a pulsed Ti:Sapphire laser. Purcell factors of up to 27, and $\beta$ factors of up to 0.89 were demonstrated; moreover, an impressive $\beta$ factor greater than 0.5 was observed over a bandwidth of 20 nm.

In the next sections, we will highlight a few chip-based schemes that can facilitate a much richer control of cavity-QED-enabled light sources. Before doing that, we make a few remarks about possible experimental bottlenecks and highlight the need for experimentalists and theorists to work together. First of all, we note that each PC sample is different, even without any QDs; so an ensemble average of measurements on nominally identical samples is needed to allow one to understand what kind of structures are being made and with what precision; following an understanding of the general dispersive, loss, and input-output characteristics, one can feed this information back into the general theoretical understanding of the device, even before QDs are embedded. Important aspects to understand include the broadened LDOS enhancements, the minimum group velocity, the finite-length dependence, and the essential role of fabrication imperfections, all of which can be added into the medium-dependent Green function. Second, comes the strategic coupling to QDs. A general ensemble of QDs can largely spoil the enhanced light-matter coupling of any PC system, and this applies to waveguides and cavities; for example, spectrally uncoupled (to the cavity mode) excitons can still radiatively couple to the environment and, for example, reduce the quality factor of the cavity. Thus the spatial positioning of a target QD, and a background ensemble of QDs can play a qualitative role. Spectrally tuning the PC system and target QD exciton is also important, and this can be achieved, for example, by gas condensation or temperature tuning; however, the latter brings about an increased influence of non-radiative decay and electron-phonon coupling. These are only a few of the important attributes; other include: input coupling, target temperature operation, entangled photon pair generation, coherent pulse generation, target wavelength operation, and so on, so we anticipate much room for improvement. Taken together, it seems that a systemic investigation is required, which will involve design and redesign, iterating towards closely matching theory and experiments in a deterministic way. Below we highlight some other approaches beyond the single cavity and single waveguide approach, that may help in this regard.

### 5.2. The "finite-size" PC waveguide

We next address the question of what happens when only a short section of a finite-size waveguide is considered, where the rigorous Bloch mode analysis and the analytical Green function techniques do not apply. In Figs. 10a and b, we show the numerically calculated spontaneous emission factors as a function of frequency for a ten unit-cell planar PC waveguide; the waveguide is bounded by, respectively, perfectly matched layers (PML) and an air medium, on both ends of the waveguide for two different

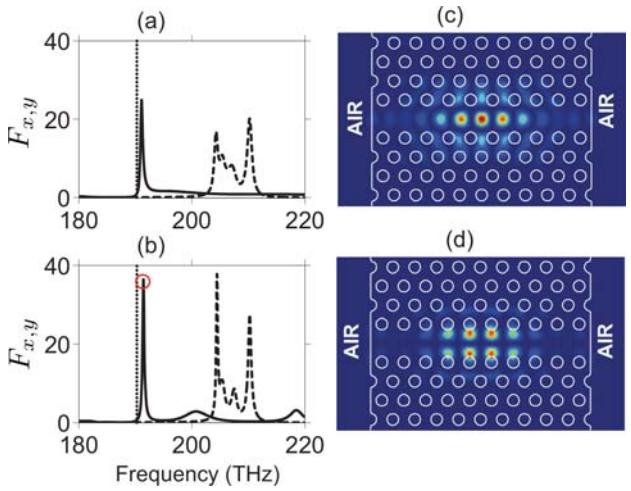


**Figure 10** (online color at: www.lpr-journal.org) (a) Purcell factors ($F$) versus frequency for a QD embedded in a 10 unit-cell finite size waveguide surrounded by PML. Dashed (solid) line is for the case when the dipole orientation of the QD is along the $x(y)$-axis, and the dotted vertical line shows the bandedge of the fundamental waveguide mode of an infinite structure. (b) Same as in (a) but with the waveguide ends surrounded by air. (c) Center of the slab contour of the $|\mathbf{f}_y|^2$ field distribution corresponding to the peak Purcell factor shown in (b), $x$-axis is along the waveguide and point to the right, $y$-axis is in plane and perpendicular to $x$-axis. (d) As in (c) but for the $|\mathbf{f}_x|^2$ component of the electric field.

dipole orientations. The PML allows light to propagate out of the sample without any reflections. Remarkably, even with only ten unit cells, a comparison of the spontaneous emission factors for both $y$- and $x$-oriented dipoles reveal all the main features of the infinite-size band structure, such as LDOS enhancements whenever the group velocity approaches zero (flat bands). With finite size, however, the band-edge divergences are significantly broadened, and also the LDOS peaks are blue shifted from the ideal band structure (shown in the figure with a vertical dotted line).

When one includes air as a surrounding medium on both sides of the PC waveguide, there is a substantial enhancement of the emission-factor ($F$), and additional spectral peaks arise due to Fabry-Perót resonances. For the LDOS peak indicated in Fig. 10b, the corresponding $y$-polarized mode ($x$-polarized mode) at the center of the slab is shown as a contour image in Fig. 10c [Fig. 10d], which yields a calculated effective mode volumes of $V_{\text{eff}} \approx 0.1\,\mu\text{m}^3$. The spatial dependence of the spontaneous emission essentially follows the spatial profile of the field modes. This suggests that QD spatial positioning within 20–40 nm will be key in achieving the predicted Purcell factor enhancements. We also highlight that these large enhancements can be achieved for both $x$- and $y$-polarization components, although the peak frequencies will be different [see solid and dashed curves in Fig. 10]. We add the following two remarks: a) the influence of the facet terminations can also play an important role [90], which could allow a systematic investigation of QD coupling as a function of sample length; and b) similar features in the PC waveguide LDOS have been observed experimentally [91].

## 6. Practical on-chip single photon sources

### *6.1. Single photon source using a PC waveguide and an output coupler*

Stimulated by the enhanced Purcell factors of a PC waveguide and efficient on-chip unidirectional collection of the emitted photons, our group has also recently proposed a "single photon gun" based on a small section of a PC waveguide near the slow-light mode, integrated with an output coupler. The coupler is based upon the design of Banaee et al. [92], and the schematic structure is shown in Fig. 11. As an example, the Purcell factor versus frequency for a 10 unit-cell waveguide in a unidirectional output is shown in Fig. 12, where the peak value is about 46. With realistic parameters, a 20 unit-cell waveguide can achieve Purcell factors of more than 200 [90]. The electric-field distribution at the peak Purcell factor (see Fig. 12) is shown in Fig. 13.

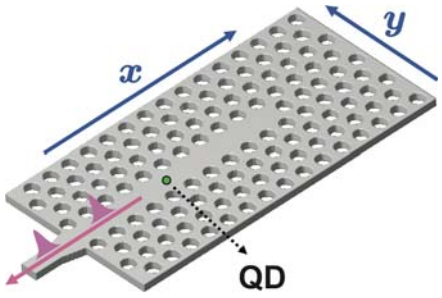


**Figure 11** (online color at: www.lpr-journal.org) Schematic diagram of a single photon source based on a finite-size PC waveguide, in the slow light regime; the green dot refers to the QD, and the target photon is emitted on-chip via the waveguide mode.

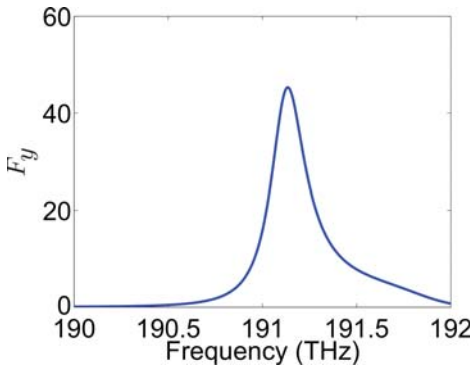


**Figure 12** (online color at: www.lpr-journal.org) Purcell factor ($F_y$) versus frequency for a QD embedded in the finite-size PC waveguide (cf. Fig. 11).

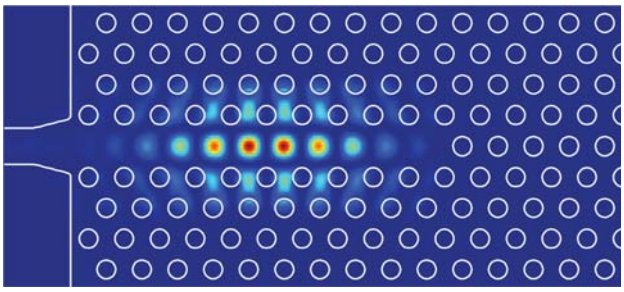

**Figure 13** (online color at: www.lpr-journal.org) The slab-center distribution of electric-field amplitude corresponding to the peak Purcell factor in Fig. 12.

With the integrated coupler, more than 60% of the emitted field overlaps with the output waveguide mode ($\beta > 0.6$). To obtain these parameters, we first calculate the ratio between the left propagating power $P_l$, at the output target waveguide (after the coupler), and the total emission power emitted by the dipole $P_t$; then a mode overlap integration is performed between the destination waveguide mode and the computed propagating electromagnetic fields, whereby the $\beta$ is the product of the overlap integration and the power ratio. Since all of these coupling parameters are not optimized, and given the complexity of single QD coupling, these numbers are already quite impressive. To put these results in context, we have nano-engineered a situation where the probability of emitting one photon with a vacuum wavelength of $\lambda = 1500$ nm, into a standard 200 nm-thick wire waveguide, is more than 60% with a significant Purcell effect.

## *6.2. Single photon source using a PC waveguide, a cavity, and an output coupler*

We next propose a device that exploits some of the advantages of integrated cavities, waveguides, and couplers. The proposed single photon source is shown schematically in Fig. 14. The parameters of the two-hole shifted cavity and the waveguide are the same as before. In this case, however, the cavity is now deliberately *over-coupled* to the PC waveguide; the PC waveguide is then coupled to an output wire waveguide.

Here, the direct 3D FDTD calculation is once more adopted. Although the Purcell factor (see Fig. 15) and the quality factor are significantly reduced in comparison with the unloaded cavity, they are still very large ($F_y \sim 1100$ and $Q \sim 10\,300$), and are one order of magnitude larger than that of the previous waveguide example; this is because of the the increased LDOS at the QD position; although the increased coupling between the cavity and the waveguide leads to the decrease of the Purcell factor compared to the bare cavity, the major advantage is that on-chip emission is possible with the integrated waveguide. The spatial distribution of the field, at the maximum Purcell

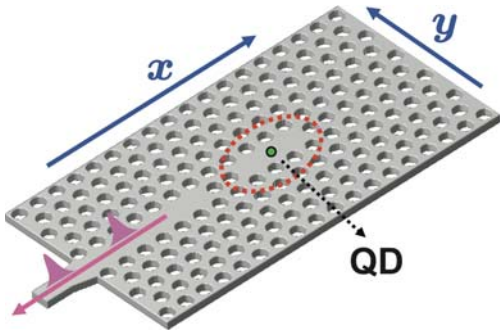


**Figure 14** (online color at: www.lpr-journal.org) Schematic diagram of waveguide-cavity single photon source, which is composed of one cavity and one waveguide, one QD (indicated by green dot) is placed within the cavity.

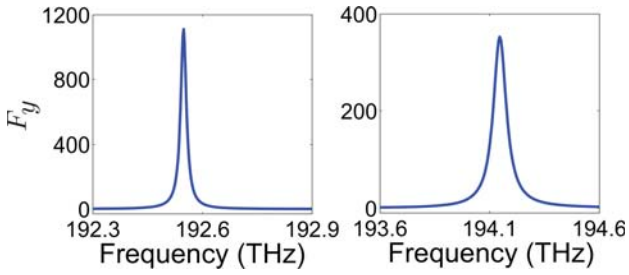


**Figure 15** (online color at: www.lpr-journal.org) Purcell factor ($F_y$) versus frequency for a QD embedded in the shifted-hole cavity (a) and no-shift cavity (b) which are "loaded" by a waveguide.

factor (see Fig. 15a), is shown in Fig. 16, which highlights how the emitted field leaks predominantly into the output waveguide. We also highlight that the peak Purcell factor is certainly larger than that required to enter the strong coupling regime for a typical QD exciton. The analytical forms of the Purcell factors, $\beta$ factor, and an investigation of the strong coupling regime is reported elsewhere [93].

Intuitively, one might imagine that the scattered light from a large-$Q/V_{\text{eff}}$ cavity will mainly escape through the vertical decay channel. But here, even with the coupling with the waveguide, the quality factor of the loaded cavity is still high (larger than 10 000); however, surprisingly, the $\beta$ factor is still as high as 50%, which is again without optimization. It can be anticipated that the collection efficiency can be further increased if we increase the coupling between waveguide and cavity, for example, by resizing or reducing the air hole radius at the interface between cavity and waveguide. We also highlight that the frequency of the peak Purcell factor now is 192.7 THz, which is strategically away from the waveguide band edge. Also, by looking at the band structure, one has a very large bandwidth with which to efficiently couple to the output waveguide propagation mode. For comparison, the no-shift cavity case is also investigated, where the peak Purcell factor is reduced to about 350, which is significantly smaller than that of

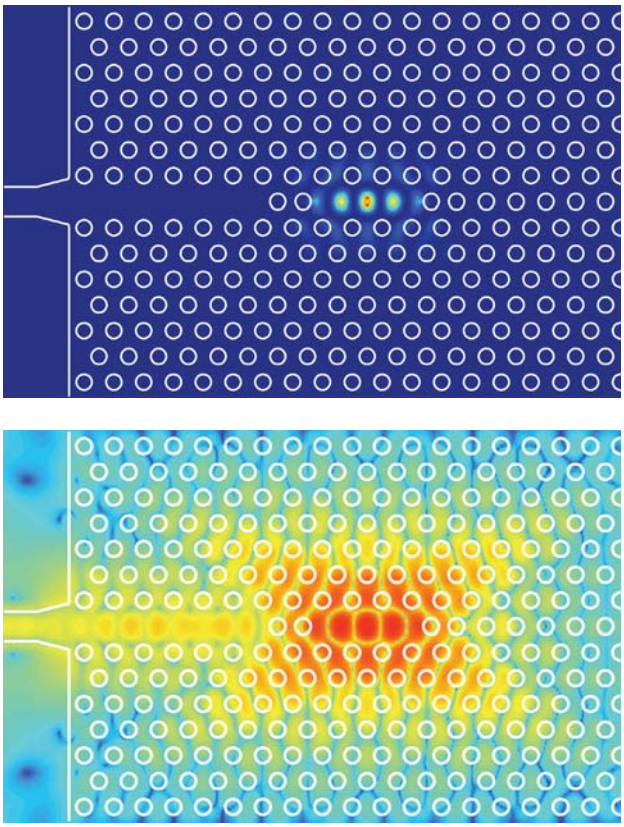

**Figure 16** (online color at: www.lpr-journal.org) The distribution of electric field amplitude, at slab center, corresponding to the peak Purcell factor in Fig. 15a, upper: linear scale, lower: log scale.

the shifted-hole case; in addition, the $\beta$ factor is only 37%, since the shifted-hole cavity has a much better coupling to the output waveguide mode, and less overlap with radiation modes above the light line; thus a large Purcell factor and a large $\beta$ factor go hand in hand for our designed structure.

## 7. Input/output relations of a PC waveguide side-coupled to a single-cavity system: single photon switching and electromagnetic induced transparency

Finally, we highlight some unique PC functionalities that can be achieved by side-coupling a cavity to a waveguide. The structure of interest is depicted in Fig. 17. To describe light propagation, we will again use a Green function approach, closely following the works of Cowan and Young [94], and Hughes and Kamada [95]. Although we show an example of just one side coupled cavity, the extension to two coupled cavities is straightforward, and can result in much richer behaviour, e.g., regimes of coupled-cavity-QED [97] and macroscopic QD entanglement [98].

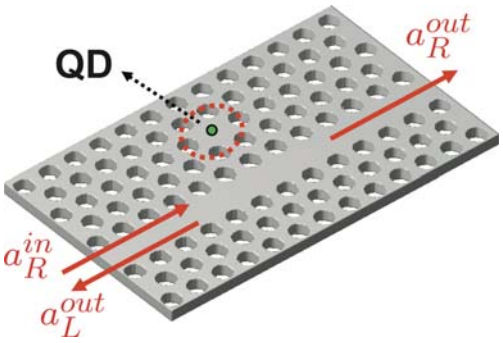


**Figure 17** (online color at: www.lpr-journal.org) Schematic diagram of semiconductor PC nanocavity side-coupled to a waveguide. The excitation field excites both the cavity and the QD, which effects the transmission and reflection of the incident field.

We briefly describe the general formalism, that directly maps on to what quantum optics researchers usually call *input/output theory*; however, this is what we would perhaps call medium-dependent scattering theory, which has been around far longer than the coined: "input/output theory". Expanding the transverse Green $\mathbf{G}_{wc}^{\mathrm{T}}$ of the PC waveguide-cavity system in terms of the cavity and waveguide eigenstates, then $\mathbf{G}_{wc}^{\mathrm{T}} = \sum_{\alpha,\beta} B_{\alpha\beta} \left|\mathbf{f}_\alpha\right\rangle \left\langle \mathbf{f}_\beta\right|$, where $\left|\mathbf{f}_\alpha\right\rangle$ are the transverse eigenmodes of the separate waveguide and cavity. From the formal definition of $\mathbf{G}_{wc}^{\mathrm{T}}$, we derive a set of equations in matrix form for the coefficients $B_{\alpha\beta}$. After solving the equation set (by matrix inversion), we obtain the full Green function expression for the waveguide-cavity system:

$$\begin{aligned}\mathbf{G}_{wc}^{\mathrm{T}} = \mathbf{G}_{w}^{\mathrm{T}} &+ \frac{\omega^2 \left|\mathbf{f}_c\right\rangle \left\langle \mathbf{f}_c\right|}{\omega_c^2 - \omega^2 - \omega^2 \left\langle \mathbf{f}_c\right| V_c \mathbf{G}_w^{\mathrm{T}} V_c \left|\mathbf{f}_c\right\rangle} \\ &+ \frac{\omega^2 \mathbf{G}_w^{\mathrm{T}} V_c \left|\mathbf{f}_c\right\rangle \left\langle \mathbf{f}_c\right|}{\omega_c^2 - \omega^2 - \omega^2 \left\langle \mathbf{f}_c\right| V_c \mathbf{G}_w^{\mathrm{T}} V_c \left|\mathbf{f}_c\right\rangle} \\ &+ \frac{\omega^2 \left|\mathbf{f}_c\right\rangle \left\langle \mathbf{f}_c\right| V_c \mathbf{G}_w^{\mathrm{T}}}{\omega_c^2 - \omega^2 - \omega^2 \left\langle \mathbf{f}_c\right| V_c \mathbf{G}_w^{\mathrm{T}} V_c \left|\mathbf{f}_c\right\rangle} \\ &+ \frac{\omega^2 \mathbf{G}_w^{\mathrm{T}} V_c \left|\mathbf{f}_c\right\rangle \left\langle \mathbf{f}_c\right| V_c \mathbf{G}_w^{\mathrm{T}}}{\omega_c^2 - \omega^2 - \omega^2 \left\langle \mathbf{f}_c\right| V_c \mathbf{G}_w^{\mathrm{T}} V_c \left|\mathbf{f}_c\right\rangle}, \end{aligned} \tag{24}$$

and since $\mathbf{K} = \mathbf{G}^{\mathrm{T}} + \sum_\lambda \frac{\varepsilon(\mathbf{r})}{\varepsilon(\mathbf{r}')} \mathbf{f}_\lambda^*(\mathbf{r}) \mathbf{f}_\lambda(\mathbf{r}')$, we can again set $\mathbf{K}_{wc} \approx \mathbf{G}_{wc}^{\mathrm{T}}$ and work exclusively with $\mathbf{G}^{\mathrm{T}}$. The shorthand notation of $V_c$, represents the perturbation in the dielectric constant that results from adding in the cavity to the perfect PC lattice [94, 95]. By subsequently exploiting the dipole approximation and the Dyson equation ($\mathbf{G}^{\mathrm{T}} = \mathbf{G}_0^{\mathrm{T}} + \mathbf{G}_0^{\mathrm{T}} V \mathbf{G}^{\mathrm{T}}$), we derive the renormalized Green function – *including the QD dot response* – as

$$\tilde{\mathbf{G}}_{wc}^{\mathrm{T}}(\mathbf{r}, \mathbf{r}', \omega) = \frac{\mathbf{G}_{wc}^{\mathrm{T}}(\mathbf{r}, \mathbf{r}', \omega)}{1 - \mathbf{n}_d \cdot \mathbf{G}_{wc}^{\mathrm{T}}(\mathbf{r}_d, \mathbf{r}_d, \omega) \cdot \mathbf{n}_d \, \alpha_0(\omega)}, \tag{25}$$

where $\alpha_0(\omega)$ is again the bare polarizability, as introduced earlier.

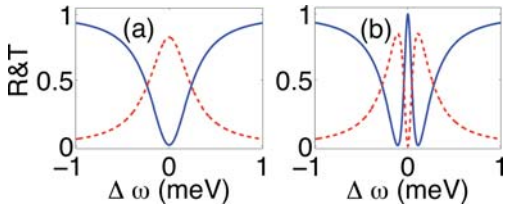


**Figure 18** (online color at: www.lpr-journal.org) Transmission (blue solid curve) and reflection (red dashed curve) of the cavity-waveguide system for the cases without (a) and with (b) a QD. The cavity-waveguide quality factor is 2000, the quality factor of bare cavity is 20 000, the effective volume is 0.07 $\mu m^3$, and the dipole moment of the QD is 50 Debye.

Equipped with the Green function of the coupled system, the problem is basically solved: we can immediately derive the input-output relations directly by simple projection. Using the Dyson solution, the total self-consistent electric field operator can be written as, $\hat{\mathbf{E}}(\omega,\mathbf{r}) \approx \hat{\mathbf{E}}_0(\omega,\mathbf{r}) + \int d\mathbf{r}'\, \tilde{\mathbf{G}}^{\mathrm{T}}_{wc}(\mathbf{r},\mathbf{r}',\omega) V_c(\mathbf{r}') \hat{\mathbf{E}}_0(\omega,\mathbf{r}')$, where $\hat{\mathbf{E}}_0(\omega,\mathbf{r})$ is the homogeneous incident-field operator to the waveguide. The field can also be defined directly through the input and output operators: $\hat{\mathbf{E}}(\omega,\mathbf{r}) = \sum_{l=L,R} \int d\nu \sqrt{\frac{\hbar\nu}{2\varepsilon_0}} \frac{\hat{a}^{\mathrm{out}}_l(\nu)}{\nu-\omega} \mathbf{f}_l(\nu,\mathbf{r}) + \mathrm{H.c.}$, where $l = L, R$ sums over the left and right output channels along the waveguide. Subsequently, assuming the incident driving field is $\hat{\mathbf{E}}_0(\omega,\mathbf{r}) = \int d\nu \sqrt{\frac{\hbar\nu}{2\varepsilon_0}} \frac{\hat{a}^{\mathrm{in}}_{l=R}(\nu)}{\nu-\omega} \mathbf{f}_R(\nu,\mathbf{r}) + \mathrm{H.c.}$, and projecting the Dyson equation onto the eigenmode $\mathbf{f}_R(\nu,\mathbf{r})$ and $\mathbf{f}_L(\nu,\mathbf{r})$, respectively, we obtain the input and output operators:

$$\hat{a}^{\mathrm{out}}_R(\omega) = \left[1 + \frac{i\omega\Gamma_c/[\omega_c^2 - \omega^2 - i\omega(\Gamma_c+\Gamma_0)]}{1 - \mathbf{n}_d \cdot \mathbf{G}^{\mathrm{T}}_{wc}(\mathbf{r}_d,\mathbf{r}_d,\omega)\cdot \mathbf{n}_d\, \alpha_0(\omega)}\right] \hat{a}^{\mathrm{in}}_R(\omega)\,, \tag{26}$$

$$\hat{a}^{\mathrm{out}}_L(\omega) = \frac{i\omega\Gamma_c/[\omega_c^2 - \omega^2 - i\omega(\Gamma_c+\Gamma_0)]}{1 - \mathbf{n}_d \cdot \mathbf{G}^{\mathrm{T}}_{wc}(\mathbf{r}_d,\mathbf{r}_d,\omega)\cdot \mathbf{n}_d\, \alpha_0(\omega)} \hat{a}^{\mathrm{in}}_R(\omega)\,, \tag{27}$$

where $\Gamma_c = \pi\omega_c^2 |\langle \mathbf{f}_c | V_c | \mathbf{f}_l \rangle|^2$, and $\Gamma_0$ is the decay rate of bare cavity. We have assumed the coupling with the left and right waveguide channel is symmetric with respect to the cavity mode. In addition, the emitted field from an excited QD exciton [96] can be obtained by projecting Eq. (9) onto the corresponding output channel, $\mathbf{f}_l(\nu,\mathbf{r})$.

In Fig. 18, we show examples of the transmission and reflection, for the systems with and without a coupled QD. The transmission and reflection are defined respectively as: $T = |\hat{a}^{\mathrm{out}}_R(\omega)/\hat{a}^{\mathrm{in}}_R(\omega)|^2$, $R = |\hat{a}^{\mathrm{out}}_L(\omega)/\hat{a}^{\mathrm{in}}_R(\omega)|^2$. The reflection case was first studied by Hughes and Kamada [95], while the transmission case was later studied by Waks et al. [99], but both approaches give essentially identical results. The *dipole-induced transparency* regime [99, 100] can be clearly seen, which is an effect that originates from the interference between the QD scattered field and the propagating input field. Interestingly, the observed splitting in the regime of dipole-induced transparency, can occur even if we are outside the regime of strong coupling; yet, within the regime of strong coupling, the spectral splitting in transmission or reflection coincides exactly with vacuum Rabi splitting [95]. The theory can also be extended to include other potentially important effects, e.g., the effect of electron-phonon coupling as a function of temperature, which demonstrates the important role of non-Markovian relaxation processes, is reported by Milde et al. [101]. Possible applications of using QD coupled waveguide systems for slow-light buffering have also been reported in [102].

## 8. Conclusions and Outlook

We have presented a brief review into the growing field of chip-based quantum light sources using planar PCs and single QDs. Since this is a large and expanding research area, we have focused on the basic physics required to design practical single photon sources using such material systems. We believe that physics-design approaches, such as those presented, offer considerably more insight than, for example, "blindly" running large-scale numerical simulations, which is perhaps too-often the current trend these days. Single photon optimization is no longer a matter of positioning a photon emitter near a field antinode, and hoping for the best; rather, key design insights and material functionalities need to be made clear. Systematic and detailed comparisons between experiments and theory are required, with and without coupled QDs. In this regard, we have discussed and applied a unified theoretical framework which can describe, predict, and design a wide variety of practical single photon emitters. A connection to the various experimental and theoretical works appearing in the recent literature has been made. This framework forms the basis for understanding the rich and complex light-matter interactions that can occur in planar PC chips, and can be extended to account for many of the things that we have chosen to leave out, such as coupled QDs, coupled cavities, electron-phonon interactions, input coupling, and entangled photon pair generation [103, 104], to name but a few.

The on-demand single photon source is an extremely important source for quantum information science and technology. As the potential suitable solid-state material of choice, we believe that the prospects for using integrated planar PC chips offer many advantages for controlling and manipulating the light-matter interactions of an embedded QD. In a remarkably short space of time, we have witnessed many impressive experiments, largely performed in an un-deterministic and heroic manner; yet, we have already seen clear evidence that planar PCs do have the ability to mutually control one photon and one electron (or one electron-hole pair) at a time. Aided by improving fabrication techniques, and by new and practical design insights, there are grounds for being optimistic in envisioning what will come next. Furthermore, because on-chip devices

can be encapsulated and reliably produced, the commercialization prospects of single photon sources using semiconductor chips will probably happen within the next five years. Having said that, one must not oversell the dream just yet! Enormous challenges remain, including the understanding and possible control of decoherence processes, the role of fabrication imperfections, as well as the ability to deterministically position single QDs, preferably working with $\lambda = 1.5\,\mu m$, within the chip. Nevertheless, we certainly envision that, in the next few years, the community will realize on-chip single photon light sources using integrated waveguide-cavity systems, such as those presented in this review.

We finish, by congratulating all the experimentalists and theorists working in the field for their continued efforts, and we look forward to see many more exciting developments in the near future.

*Acknowledgements* We thank Robin Williams, Jeff Young, Pradyumna Pathak, and Martijn Wubs for useful discussions. This work was supported by the National Sciences and Engineering Research Council of Canada, and the Canadian Foundation for Innovation.

Peijun Yao received his B. Sc. and Ph. D. degrees in physics from University of Science and Technology of China, Hefei in 2000 and 2005 respectively. After his thesis work on the design and simulation of photonic crystal devices, he was a researcher at the Shanghai Institute of Microsystem and Information Technology. From 2008, he has been a postdoctoral fellow at Queen's University, Canada. His current research interests include light-matter interaction effects of quantum dots embedded in planar photonic crystals and photonic metamaterials.

Manga Rao received his B. Sc. and M. Sc. in Physics from Sri Sathya Sai University, India in 1998 and 2000, and his Ph. D. degree in Physics from University of Hyderabad, India in 2006. During 2006–2007 he was a postdoctoral fellow at Queen's University, Canada, and in 2008, he worked in UTINAM-UMR CNRS, France. Presently, he is a researcher in the Nanoscience Laboratory at the University of Trento, Italy, involved in the design and simulation of on-chip photonic devices for optical networks and biosensors. His current research interests include silicon and hybrid photonics and integrated photonic circuits.

Stephen Hughes received the B. Sc. and Ph. D. degrees in physics from Heriot-Watt University, Edinburgh in 1991 and 1995, respectively. Following Postdoctoral Fellowships at Philipps-University Marburg (Germany), the University of Tokyo (Japan), and Washington State University (USA), he became a Lecturer of Physics at the University of Surrey, UK. In 2001, he joined the first photonics start-up company to explore the commercialization of planar photonic crystals, Galian Photonics Inc., in Vancouver, BC, Canada. Subsequently he co-founded a new optical software company, Lumerical Solutions Inc., and then spent two years at NTT Basic Research Laboratories, Japan, as a Research Specialist. He returned to Canada in 2005 to take up the position of Associate Professor at Queen's University. His research group carries out a wide range of theoretical and computational investigations of light-matter interaction processes in photonic nanostructures, and explores the consequences of these for next-generation technologies.

## References

[1] C. H. Bennett and D. P. Divincenzo, Quantum information and computation, Nature **404**, 247 (2000).
[2] N. Gisin, G. Ribordy, W. Tittel, and H. Zbinden, Quantum cryptography, Rev. Mod. Phys. **74**, 145 (2002).
[3] N. Gisin and R. Thew, Quantum communication, Nature Photonics **1**, 165 (2007).
[4] B. Lounis and M. Orrit, Single-photon sources, Rep. Prog. Phys. **68**, 1129 (2005).
[5] A. Muller, T. Herzog, B. Huttner, W. Tittel, H. Zbinden, and N. Gisin, Plug and play systems for quantum cryptography, Appl. Phys. Lett. **70**, 793 (1997).
[6] G. Brassard, N. Lütkenhaus, T. Mor, and B. C. Sanders, Limitations on practical quantum cryptography, Phys. Rev. Lett. **85**, 1330 (2000).
[7] N. Lütkenhaus, Security against individual attacks for realistic quantum key distribution, Phys. Rev. A **61**, 052304 (2000).
[8] S. A. Castelletto and R. E. Scholten, Heralded single photon sources: a route towards quantum communication technology and photon standards, Eur. Phys. J. Appl. Phys. **41**, 181 (2008).
[9] H. J. Kimble, M. Dagenais, and L. Mandel, Photon antibunching in resonance fluorescence, Phys. Rev. Lett. **39**, 691 (1977).
[10] A. Kuhn, M. Hennrich, and G. Rempe, Deterministic single-Photon source for distributed quantum networking, Phys. Rev. Lett. **89**, 067901 (2002).
[11] M. Keller, B. Lange, K. Hayasaka, W. Lange, and H. Walther, Continuous generation of single photons with controlled waveform in an ion-trap cavity system, Nature **431**, 1075 (2004).

[12] C. Brunel, B. Lounis, P. Tamarat, and M. Orrit, Triggered source of single photons based on controlled single molecule fluorescence, Phys. Rev. Lett. **83**, 2722 (1999).
[13] B. Lounis and W. E. Moerner, Single photons on demand from a single molecule at room temperature, Nature **407**, 491 (2000).
[14] C. Kurtsiefer, S. Mayer, P. Zarda, and H. Weinfurter, Stable solid-state source of single photons, Phys. Rev. Lett. **85**, 290 (2000).
[15] Z. Yuan, B. E. Kardynal, R. M. Stevenson, A. J. Shields, C. J. Lobo, K. Cooper, N. S. Beattie, D. A. Ritchie, and M. Pepper, Electrically driven single-photon source, Science **295**, 102 (2002).
[16] W. Chang, W. Chen, H. Chang, T. Hsieh, J. Chyi, and T. Hsu, Efficient single-photon sources based on low-density quantum dots in photonic-crystal nanocavities, Phys. Rev. Lett. **96**, 117401 (2006).
[17] A. Badolato, K. Hennessy, M. Atatüre, J. Dreiser, E. Hu, P. M. Petroff, and A. Imamoğlu, Deterministic Coupling of single quantum dots to single nanocavity modes, Science **308**, 1158 (2005).
[18] P. Michler, A. Kiraz, C. Becher, W. V. Schoenfeld, P. M. Petroff, Lidong Zhang, E. Hu, and A. Imamoğlu, A quantum dot single-photon turnstile device, Science **290**, 2282 (2000).
[19] E. Yablonovitch, Inhibited Spontaneous Emission in Solid-State Physics and Electronics, Phys. Rev. Lett. **58**, 2059 (1987)
[20] S. John, Strong localization of photons in certain disordered dielectric superlattices, Phys. Rev. Lett. **58**, 2486 (1987).
[21] P. Borri, W. Langbein, S. Schneider, U. Woggon, R. L. Sellin, D. Ouyang, and D. Bimberg, Ultralong dephasing time in InGaAs quantum dots, Phys. Rev. Lett. **87**, 157401 (2001).
[22] T. H. Stievater, Xiaoqin Li1, D. G. Steel, D. Gammon, D. S. Katzer, D. Park, C. Piermarocchi, and L. J. Sham, Rabi oscillations of excitons in single quantum dots, Phys. Rev. Lett. **87**, 133603 (2001).
[23] H. Kamada, H. Gotoh, J. Temmyo, T. Takagahara, and H. Ando, Exciton rabi oscillation in a single quantum dot, Phys. Rev. Lett. **87**, 246401 (2001).
[24] T. Takagahara, Theory of exciton dephasing in semiconductor quantum dots, Phys. Rev. B **60**, 2638 (1999).
[25] A. Vagov, V. M. Axt, and T. Kuhn, Electron-phonon dynamics in optically excited quantum dots: Exact solution for multiple ultrashort laser pulses, Phys. Rev. B **66**, 165312 (2002).
[26] J. Förstner, C. Weber, J. Danckwerts, and A. Knorr, Phonon-assisted damping of Rabi oscillations in semiconductor quantum dots, Phys. Rev. Lett. **91**, 127401 (2003).
[27] E. A. Muljarov and R. Zimmermann, Dephasing in quantum dots: quadratic coupling to acoustic phonons, Phys. Rev. Lett. **93**, 237401 (2004).
[28] E. M. Purcell, Spontaneous emission probabilities at radio frequencies, Phys. Rev. **69**, 681 (1946).
[29] E. Moreau, I. Robert, J. M. Gérard, I. Abram, L. Manin, and V. Thierry-Mieg, Single-mode solid-state single photon source based on isolated quantum dots in pillar microcavities, Appl. Phys. Lett. **79**, 2865 (2001).
[30] C. Santori, D. Fattal, J. Vučković, G. S. Solomon, and Y. Yamamoto, Indistinguishable photons from a single-photon device, Nature **419**, 594 (2002).
[31] M. Pelton, C. Santori, J. Vučković, B. Zhang, G. S. Solomon, J. Plant, and Y. Yamamoto, Efficient source of single photons: a single quantum dot in a micropost microcavity, Phys. Rev. Lett. **89**, 233602 (2002).
[32] C. Santori, M. Pelton, C. Solomon, Y. Dale, and Y. Yamamoto, Triggered single photons from a quantum dot, Phys. Rev. Lett. **86**, 1502 (2001).
[33] P. Michler, A. Kiraz, L. Zhang, C. Becher, E. Hu, and A. A. Imamoğlu, Laser emission from quantum dots in microdisk structures, Appl. Phys. Lett. **77**, 184 (2000).
[34] M. O. Scully and M. S. Zubairy, Quantum Optics (Cambridge University Press, Cambridge, 1997).
[35] R. Loudon, The Quantum Theory of Light, third ed. (Oxford University Press, New York, 2004).
[36] R. Hanbury Brown and R. Q. Twiss, Correlation between photons in 2 coherent beams of light, Nature **177**, 27 (1956).
[37] R. Hanbury Brown and R. Q. Twiss, Interferometry of the intensity fluctuations in light; II. An experimental test of the theory for partially coherent light, Proc. R. Soc. A **243**, 291 (1957).
[38] M. Wubs, L. G. Suttorp, and A. Lagendijk, Multiple-scattering approach to interatomic interactions and superradiance in inhomogeneous dielectrics, Phys. Rev. A **70**, 053823 (2004).
[39] N. Vats, S. John, and K. Busch, Theory of fluorescence in photonic crystals, Phys. Rev. A **65**, 043808 (2002).
[40] H. J. Carmichael, R. J. Brecha, M. G. Raizen, and H. J. Kimble, Subnatural linewidth averaging for coupled atomic and cavity-mode oscillators, Phys. Rev. A **40**, 5516 (1989).
[41] H. J. Carmichael, Statistical Methods in Quantum Optics 2 (Springer, Berlin, Heidelberg, New York, 2008).
[42] L. C. Andreani, G. Panzarini, and J.-M. Gérard, Strong-coupling regime for quantum boxes in pillar microcavities: Theory, Phys. Rev. B **60**, 13276 (1999);
[43] H. T. Dung, S. Scheel, D.-G. Welsch, and L. Knöll, J. Opt. B **4**,169 (2002).
[44] H. T. Dung, L. Knöll, and D.-G. Welsch, Phys. Rev. A **62**, 053804 (2000).
[45] H. A. Bethe, The electromagnetic shift of energy levels, Phys. Rev. **72**, 339 (1947).
[46] Y. Akahane, T. Asano, B. Song, and S. Noda, High-Q photonic nanocavity in a two-dimensional photonic crystal, Nature **425**, 944 (2003).
[47] T. Yoshie, A. Scherer, J. Hendrickson, G. Khitrova, H. M. Gibbs, G. Rupper, C. Ell, O. B. Shchekin, and D. G. Deppe, Vacuum Rabi splitting with a single quantum dot in a photonic crystal nanocavity, Nature **432**, 200 (2004).
[48] A. Kress, F. Hofbauer, N. Reinelt, M. Kaniber, H. J. Krenner, R. Meyer, G. Böhm, and J. J. Finley, Manipulation of the spontaneous emission dynamics of quantum dots in two-dimensional photonic crystals, Phys. Rev. B **71**, 241304(R) (2005).
[49] D. Englund, D. Fattal, E. Waks, G. Solomon, B. Zhang, T. Nakaoka, Y. Arakawa, Y. Yamamoto, and J. Vučković, Controlling the Spontaneous Emission Rate of Single Quantum Dots in a Two-Dimensional Photonic Crystal, Phys. Rev. Lett. **95**, 013904 (2005).
[50] K. Hennessy, A. Badolato, M. Winger, D. Gerace, M. Atatüre, S. Gulde, S. Fält, E. L. Hu, and A. Imamoğlu,

Quantum nature of a strongly coupled single quantum dot-cavity system, Nature **445**, 896 (2007).
[51] S. Frédérick, D. Dalacu, J. Lapointe, P. J. Poole, G. C. Aers, and R. L. Williams, Experimental demonstration of high quality factor, x-dipole modes in InAs/InP quantum dot photonic crystal microcavity membranes, Appl. Phys. Lett. **89**, 091115 (2006).
[52] S. Combrié, A. D. Rossi, Q. V. Tran, and H. Benisty, GaAs photonic crystal cavity with ultrahigh Q: microwatt nonlinearity at 1.55 μm, Opt. Lett. **33**, 1908 (2008).
[53] V. S. C. Manga Rao and S. Hughes, Single quantum dot spontaneous emission in a finite-size photonic crystal waveguide: Proposal for an efficient "on chip" single photon gun, Phys. Rev. Lett. **99**, 193901 (2007).
[54] A. Taflove and S. C. Hagness, Computational Electrodynamics: The Finite-Difference Time-Domain Method, 3rd ed. (Artech House, Norwood, MA, 2005).
[55] S. Hughes, Quantum emission dynamics from a single quantum dot in a planar photonic crystal nanocavity, Opt. Lett. **30**, 1393 (2005).
[56] S. Hughes and P. Yao, Theory of the quantum nature of a strongly coupled single quantum dot cavity system, Opt. Express **17**, 3322 (2009).
[57] T. Asano, B.-S. Song, and S. Noda, Analysis of the experimental Q factors (∼ 1 million) of photonic crystal nanocavities, Opt. Express **14**, 1996 (2006).
[58] D. Gerace and L. C. Andreani, Photonics and Nanostructures **3**, 120 (2005).
[59] D. P. Fussell, S. Hughes, and M. M. Dignam, Influence of fabrication disorder on the optical properties of coupled-cavity photonic crystal waveguides, Phys. Rev. B **78**, 144201 (2008).
[60] L. Ramunno and S. Hughes, Disorder-induced resonance shifts in high-index-contrast photonic crystal nanocavities, Phys. Rev. B **79**, 161303(R), (2009).
[61] E. Illes, P. Yao, and S. Hughes, Unusual quantum correlations and photon antibunching in an off-resonant quantum dot photonic-crystal cavity system, paper ITuJ3, CLEO/IQEC, Baltimore, 2009; E. Illes and S. Hughes, Antibunching correlations in a strongly coupled exciton photonic crystal cavity system: role of off-resonant coupling to multiple excitons, submitted; see arXiv:0906.4532v1 [cond-mat.mes-hall].
[62] A. Auffeves, B. Besga, J.-M. Gérard, and J.-P. Poizat, Spontaneous emission spectrum of a two-level atom in a very-high-Q cavity, Phys. Rev. A **77**, 063833 (2008).
[63] M. Yamaguchi, T. Asano, and S. Noda, Photon emission by nanocavity-enhanced quantum anti-Zeno effect in solid-state cavity quantum-electrodynamics, Opt. Express **16**, 18067 (2008).
[64] A. Naesby, T. Suhr, P. T. Kristensen, and J. Mørk, Influence of pure dephasing on emission spectra from single photon sources, Phys. Rev. A **78**, 045802 (2008).
[65] B. Song, S. Noda, and T. Asano, Photonic devices based on in-plane hetero photonic crystals, Science **300**, 1537 (2003).
[66] M. Thorhauge, L. H. Frandsen, and P. I. Borel, Efficient photonic crystal directional couplers, Opt. Lett. **28**, 1525 (2003).
[67] S. Fan, P. R. Villeneuve, J. D. Joannopoulos, and H. A. Haus, Channel drop tunneling through localized states, Phys. Rev. Lett. **80**, 960 (1998).
[68] L. Wu, M. Mazilu, J. F. Gallet, T. F. Krauss, A. Jugessur, and R. M. De La Rue, Planar photonic crystal polarization splitter, Opt. Lett. **29**, 1620 (2004).
[69] D. Kleppner, Inhibited spontaneous emission, Phys. Rev. Lett. **47**, 233 (1981).
[70] G. Lecamp, P. Lalanne, and J. P. Hugonin, The electromagnetic properties of light emission into semiconductor waveguides, Proc. SPIE **6195**, 61950E (2006).
[71] S. Hughes, Enhanced single-photon emission from quantum dots in photonic crystal waveguides and nanocavities, Opt. Lett. **29**, 2659 (2004).
[72] M. Notomi, K. Yamada, A. Shinya, J. Takahashi, C. Takahashi, and I. Yokohama, Extremely large group-velocity dispersion of line-defect waveguides in photonic crystal slabs, Phys. Rev. Lett. **87**, 253902 (2001).
[73] Y. A. Vlasov, M. O'boyle, H. F. Hamann, and S. J. Mcnab, Active control of slow light on a chip with photonic crystal waveguides, Nature **438**, 65 (2005).
[74] T. Baba, Slow light in photonic crystals, Nature Photonics **2**, 465 (2008).
[75] S. Hughes, L. Ramunno, J. F. Young, and J. E. Sipe, Extrinsic optical scattering loss in photonic crystal waveguides: role of fabrication disorder and photon group velocity, Phys. Rev. Lett. **94**, 033903 (2005).
[76] M. L. Povinelli, S. G. Johnson, E. Lidorikis, and J. D. Joannopoulos, and Marin Soljačić, Effect of a photonic band gap on scattering from waveguide disorder, App. Phys. Lett. **84**, 3639 (2004).
[77] D. Gerace and L. C. Andreani, Disorder-induced losses in photonic crystal waveguides with line defects, Opt. Lett. **29**, 1897 (2004).
[78] E. Kuramochi, M. Notomi, S. Hughes, A. Shinya, T. Watanabe, and L. Ramunno, Disorder-induced scattering loss of line-defect waveguides in photonic crystal slabs, Phys. Rev. B **72**, 161318 (2005).
[79] L. O'Faolain, T. P. White, D. O'Brien, X. Yuan, M. D. Settle, and T. F. Krauss, Dependence of extrinsic loss on group velocity in photonic crystal waveguides, Opt. Express **15**, 13129 (2007).
[80] R. J. P. Engelen, D. Mori, T. Baba, and L. Kuipers, Two regimes of slow-light losses revealed by adiabatic reduction of group velocity, Phys. Rev. Lett. **101**, 103901 (2008).
[81] J. G. Pedersen, S. Xiao, and N. A. Mortensen, Limits of slow light in photonic crystals, Phys. Rev. B **78**, 153101 (2008).
[82] M. Patterson, S. Hughes, S. Combrié, N.-V.-Quynh Tran, A. De Rossi, R. Gabet, and Y. Jaouën, Disorder-induced coherent scattering in slow-light photonic crystal waveguides, Phys. Rev. Lett. **102**, 253903 (2009).
[83] V. S. C. Manga Rao and S. Hughes, Single quantum-dot Purcell factor and beta factor in a photonic crystal waveguide, Phys. Rev. B **75**, 205437 (2007).
[84] E. Kuramochi, M. Notomi, S. Mitsugi, A. Shinya, T. Tanabe, and T. Watanabe, Ultrahigh-Q photonic crystal nanocavities realized by the local width modulation of a line defect, Appl. Phys. Lett. **88**, 041112 (2006).
[85] Y. A. Vlasov, M. O. Boyle, H. F. Hamann, and S. J. McNab, Active control of slow light on a chip with photonic crystal waveguides, Nature **438**, 65 (2005).
[86] G. Lecamp, P. Lalanne, and J. P. Hugonin, Very large spontaneous-emission factors in photonic-crystal waveguides, Phys. Rev. Lett. **99**, 023902 (2007).

[87] D. P. Fussell and M. M. Dignam, Quantum-dot-photon dynamics in a coupled-cavity waveguide: observing bandedge quantum optics, Phys. Rev. A **76**, 053801 (2007).
[88] E. Viasnoff-Schwoob, C. Weisbuch, H. Benisty, S. Olivier, S. Varoutsis, I. Robert-Philip, R. Houdré, and C. J. M. Smith, Spontaneous emission enhancement of quantum dots in a photonic crystal wire, Phys. Rev. Lett. **95**, 183901 (2005).
[89] T. Lund-Hansen, S. Stobbe, B. Julsgaard, H. Thyrrestrup, T. Sünner, M. Kamp, A. Forchel, and P. Lodahl, Experimental realization of highly efficient broadband coupling of single quantum dots to a photonic crystal waveguide, Phys. Rev. Lett. **101**, 113903 (2008).
[90] V. S. C. Manga Rao and S. Hughes, Numerical study of exact Purcell factors in finite-size planar photonic crystal waveguides, Opt. Lett. **33**, 1587 (2008).
[91] X. Letartre, C. Seassal, C. Grillet, P. Rojo-Romeo, P. Viktorovitch, and M. Le Vassor, d'Yerville, D. Cassagne, and C. Jouanin, Group velocity and propagation losses measurement in a single-line photonic-crystal waveguide on InP membranes, Appl. Phys. Lett. **79**, 2312 (2001).
[92] M. G. Banaee, A. G. Pattantyus-Abraham, M. W. McCutcheon, G. W. Rieger, and J. F. Young, Efficient coupling of photonic crystal microcavity modes to a ridge waveguide, Appl. Phys. Lett. **90**, 193106 (2007).
[93] P. Yao and S. Hughes, Controlled cavity-QED using a planar photonic crystal waveguide-cavity system, submitted; see arXiv:0904.4469v2 [physics.optics].
[94] A. Cowan and J. E. Young, Optical bistability involving photonic crystal microcavities and Fano line shapes, Phys. Rev. E **68**, 046606 (2003).
[95] S. Hughes and H. Kamada, Single-quantum-dot strong coupling in a semiconductor photonic crystal nanocavity side coupled to a waveguide, Phys. Rev. B **70**, 195313 (2004).
[96] D. P. Fussell and M. M. Dignam, Spontaneous emission in coupled microcavity-waveguide structures at the band edge, Opt. Lett. **32**, 1527 (2007).
[97] S. Hughes, Coupled-cavity qed using planar photonic crystals, Phys. Rev. Lett. **98**, 083603 (2007)
[98] P. Yao and S. Hughes, Macroscopic entanglement and violation of Bell's inequalities between two spatially separated quantum dots in a planar photonic crystal, Opt. Express **17**, 11505 (2009).
[99] E. Waks and J. Vuckovic, Dipole induced transparency in drop-filter cavity-waveguide systems, Phys. Rev. Lett. **96**, 153601 (2006).
[100] A. Auffèves-Garnier, C. Simon, J.-M. Gérard, and J.-P. Poizat, Giant optical nonlinearity induced by a single two-level system interacting with a cavity in the Purcell regime, Phys. Rev. A **75**, 053823 (2007).
[101] F. Milde, A. Knorr, and S. Hughes, Role of electron-phonon scattering on the vacuum Rabi splitting of a single-quantum dot and a photonic-crystal-nanocavity, Phys. Rev. B **78**, 035330 (2008).
[102] V. S. C. Manga Rao and S. Hughes, Single quantum dots for slow and fast light control in a planar photonic crystal, Opt. Lett. **32**, 304 (2007).
[103] R. Johne, N. A. Gippius, G. Pavlovic, D. D. Solnyshkov, I. A. Shelykh, and G. Malpuech, Entangled photon pairs produced by a quantum dot strongly coupled to a microcavity, Phys. Rev. Lett. **100**, 240404 (2008).
[104] P. K. Pathak and S. Hughes, Generation of entangled photon pairs from a single quantum dot embedded in a planar photonic-crystal cavity, Phys. Rev. B **79**, 205416 (2009).